

Fast Embedding for JOFC Using the Raw Stress Criterion

Vince Lyzinski*

Johns Hopkins University Human Language Technology Center of Excellence,
Youngser Park

Center for Imaging Sciences, Johns Hopkins University,
Carey E. Priebe

Department of Applied Mathematics and Statistics, Johns Hopkins University,
and

Michael Trosset

Department of Statistics, Indiana University

November 1, 2016

Abstract

The Joint Optimization of Fidelity and Commensurability (JOFC) manifold matching methodology embeds an omnibus dissimilarity matrix consisting of multiple dissimilarities on the same set of objects. One approach to this embedding optimizes the preservation of fidelity to each individual dissimilarity matrix together with commensurability of each given observation across modalities via iterative majorization of a raw stress error criterion by successive Guttman transforms. In this paper, we exploit the special structure inherent to JOFC to exactly and efficiently compute the successive Guttman transforms, and as a result we are able to greatly speed up the JOFC procedure for both in-sample and out-of-sample embedding. We demonstrate the scalability of our implementation on both real and simulated data examples.

Keywords: Multidimensional Scaling, manifold matching, distance geometry, distance matrices

*The authors gratefully acknowledge support from the XDATA program of the Defense Advanced Research Projects Agency (DARPA) administered through Air Force Research Laboratory contract FA8750-12-2-0303, and the NSF BRAIN Early Concept Grants for Exploratory Research (EAGER) award DBI-1451081.

1 Introduction and Background

Manifold matching—embedding multiple modality data sets into a common low-dimensional space wherein joint inference can be investigated—is an important inference task in statistical pattern recognition, with applications in computer vision (see, for example, Nastar et al., 1996; Hardoon et al., 2004; Elgammal and Lee, 2004; Wang and Suter, 2007; Ham et al., 2003), text and language processing (see, for example, Karakos et al., 2007; Vinokourov et al., 2002; Sahami and Heilman, 2006), and machine learning (see, for example, Wang and Mahadevan, 2008, 2009; Lafon et al., 2006; Ham et al., 2005), to name a few; for a survey of the literature on manifold matching and the broader problem of transfer learning, see Pan and Yang (2010).

In the present manifold matching framework, we consider n objects, each measured under m disparate modalities or conditions, each modality yielding an object-wise dissimilarity matrix $\{\Delta_i\}_{i=1}^m$; thus $\Delta_1, \Delta_2, \dots, \Delta_m \in \mathbb{R}_+^{n \times n}$. The Joint Optimization of Fidelity and Commensurability (JOFC) algorithm of Priebe et al. (2013) is a manifold matching procedure that simultaneously embeds these mn data points (n objects in m modalities) into a common Euclidean space by embedding an omnibus dissimilarity matrix $\mathbf{\Delta}$ which encapsulates the information contained in the dissimilarities $\{\Delta_i\}_{i=1}^m$. The JOFC algorithm has proven to be a flexible and effective manifold matching algorithm, with numerous applications and extensions in the literature; see Ma et al. (2012); Sun and Priebe (2013); Lyzinski et al. (2013); Adali and Priebe (2015); Shen et al. (2016). One approach to this embedding optimizes the preservation of fidelity to each individual dissimilarity matrix (i.e., preserving the within modality dissimilarities) together with the commensurability of the observations across modalities (i.e., preserving the cross-modality matchedness of the data). This approach embeds $\mathbf{\Delta}$ by minimizing Kruskal’s raw stress criterion for metric multidimensional scaling (MDS) via successive Guttman transforms (Borg and Groenen, 2005); see Algorithm 1.

In this paper, we exploit the special structure of the JOFC weight matrix to exactly and efficiently compute these successive Guttman transforms. Employing this and further computational simplifications, we are able to dramatically speed the JOFC procedure (see Algorithm 2) and extend this speedup to out-of-sample embedding for JOFC. In addition,

Notation	Description	Reference
J_n	The $n \times n$ matrix of all 1's	Used throughout
I_n	The $n \times n$ identity matrix	Used throughout
\mathbf{X}	Final configuration obtained via 3-RSMDS JOFC and fJOFC	Sec. 1.2, 1.2.1 and 2
$\tilde{\sigma}(\mathbf{X})$	The raw stress objective fcn. of 3-RSMDS	Eq. (1)
$\tilde{\Delta}$	The omnibus dissimilarity embedded by 3-RSMDS	Eq. (2)
$\sigma(\mathbf{X})$	The raw stress objective fcn. of JOFC and fJOFC	Eq. (3)
Δ	The omnibus dissimilarity embedded by JOFC and fJOFC	Eq. (5)
\mathbf{W}	The weight matrix used in the JOFC and fJOFC embeddings	Eq. (6)
\mathbf{L}	The combinatorial Laplacian of \mathbf{W}	Sec. 1.2.1 and 2
$B(\mathbf{X})$	The B -matrix used in the JOFC Guttman transform updates	Eq. (7)
\mathbf{L}^\dagger	The Moore-Penrose pseudoinverse of \mathbf{L}	Sec. 1.2.1 and 2
\mathcal{W}	A modified weight matrix used in the computation of \mathbf{L}^\dagger	Eq. (10)
$\Delta^{(o)}$	The out-of-sample omnibus dissimilarity embedded by fJOFC	Sec. 3
$\sigma_{\mathbf{x}}(\mathbf{y})$	The out-of-sample raw stress criterion	Sec. 3
$\mathbf{W}^{(o)}$	The out-of-sample weight matrix used in the fJOFC embedding	Sec. 3
$\mathbf{L}^{(o)}$	The combinatorial Laplacian of $\mathbf{W}^{(o)}$	Sec. 3

Table 1: Table of relevant notation.

parallelizing the resulting algorithm—see Remark 8—is immediate. We demonstrate these speedups and the utility of the JOFC framework in real and synthetic data examples.

Notation: To aid the reader, we have collected the frequently used notation introduced in this manuscript into a table for ease of reference; see Table 1.

1.1 JOFC and Three-Way Raw Stress MDS

In the JOFC framework, we use Raw Stress MDS to simultaneously embed the m object-wise dissimilarity matrices $\Delta_1, \Delta_2, \dots, \Delta_m \in \mathbb{R}_+^{n \times n}$ while preserving both the matchedness of the objects across modality and the within modality dissimilarities. In this way, JOFC is closely related to Three-Way Raw Stress MDS (3-RSMDS). The key difference is that

the cross modality matchedness of the objects in 3-RSMDS is enforced via a constraint on the feasible region, while in JOFC the matchedness is enforced by adding a suitable term into the raw stress criterion. In that light, JOFC can be viewed as a softly constrained version of 3-RSMDS. We highlight the commonalities and differences between the two approaches below, and in Section 4.1 empirically compare their respective performances in an illustrative simulation. For further discussion of the connection between JOFC and Three-Way Nonmetric MDS in the context of hypothesis testing, see Castle (2012), Chapter 8.

Remark 1. While the JOFC algorithm is closely related to 3-RSMDS, it bears mentioning the relationship of the algorithm to other existing manifold alignment procedures. Many existing algorithms begin with a set of high-dimensional points sampled or observed from manifolds in \mathbb{R}^k ; see, for example, Ham et al. (2005); Wang and Suter (2007); Sharma et al. (2012). Dimension reduction techniques are then applied jointly to the observations to align the manifolds in a common d -dimensional embedding space with $d \ll k$. In JOFC—similar to many of MDS and kernel based methods; see, for example, Leeuw and Mair (2008); Wang and Mahadevan (2008); Shen et al. (2016)—often the objects’ measurements cannot be made in Euclidean space. For example, the views of a single object may represent the i. text content, ii. images, iii. communication activity associated with a single social media profile. While these data are non-Euclidean by nature, nonetheless there are well established dissimilarities that can be computed within each modality. Indeed, the only requirement in the JOFC framework is that we can compute dissimilarities amongst the data points *within* each modality.

1.2 Three-Way Raw Stress MDS

In both the 3-RSMDS and the JOFC frameworks, we seek to simultaneously embed the m object-wise dissimilarity matrices, and in both regimes, the m dissimilarities are measured between the same n objects; i.e., they are produced by repeated measurements or observations under potentially disparate modalities. Assuming that the entire cross-modality correspondence is known *a priori* between the n objects, *Three-Way Raw Stress Multidi-*

mensional Scaling (3-RSMDS) seeks to find a configuration

$$\mathbf{X}^\top = [(\mathbf{X}^{(1)})^\top | (\mathbf{X}^{(2)})^\top | \dots | (\mathbf{X}^{(m)})^\top] \in \mathbb{R}^{mn \times d},$$

of the mn points that minimizes the raw stress criterion,

$$\tilde{\sigma}(\mathbf{X}) = \sum_{i=1}^m \sum_{j < k} ([\Delta_i]_{j,k} - d_{j,k}(\mathbf{X}^{(i)}))^2, \quad (1)$$

subject to the constraint that $\mathbf{X}^{(i)} = \mathbf{G}\mathbf{W}^{(i)}$ for all $i \in [m] := \{1, 2, \dots, m\}$ (note that to remove nonidentifiability issues, \mathbf{G} is often constrained to satisfy $\mathbf{G}\mathbf{G}^\top = I_n$). In (1), for $\mathbf{M} \in \mathbb{R}^{k \times \ell}$, $d_{i,j}(\mathbf{M})$ is the Euclidean distance between the i -th and j -th rows of \mathbf{M} , and for $i \in [n]$, $\mathbf{X}^{(i)}$ are the embedded points in \mathbb{R}^d corresponding to Δ_i . Adopting the terminology in Borg and Groenen (2005), in the dimension-weighting 3-RSMDS model, \mathbf{G} is known as the *group stimulus space*, and the $\mathbf{W}^{(i)}$ are diagonal matrices with nonnegative diagonal entries. In this model, the individual embeddings $\mathbf{X}^{(i)}$ differ only in the (potentially different) weights—given by the diagonal entries of the respective $\mathbf{W}^{(i)}$'s—they place on the dimensions of \mathbf{G} .

The 3-RSMDS dimension weighting model and its variants have been well-studied in the literature; see, for example, Carroll and Chang (1970); Carroll and Wish (1974); Schulz (1980); De Leeuw and Heiser (1980); Heiser (1988); Harshman and Lundy (1984). Indeed, there are a number of proposed procedures in the literature for solving the Three-Way MDS problem under a variety of error criterion, including the INDSCAL algorithm of Carroll and Chang (1970); the IDIOSCAL algorithm of Carroll and Wish (1974); Schulz (1980); the PROXSCAL algorithm of Heiser (1988); and the PARAFAC algorithm of Harshman and Lundy (1984); among numerous others. We note here that minimizing (1) subject to the constraint $\mathbf{X}^{(i)} = \mathbf{G}\mathbf{W}^{(i)}$ for all $i \in \{1, 2, \dots, m\}$ is equivalent to performing constrained Raw Stress MDS on the dissimilarity matrix

$$\tilde{\Delta} = \begin{bmatrix} \Delta_1 & \text{NA} & \cdots & \text{NA} \\ \text{NA} & \Delta_2 & \cdots & \text{NA} \\ \vdots & \vdots & \ddots & \vdots \\ \text{NA} & \text{NA} & \cdots & \Delta_m \end{bmatrix} \in \mathbb{R}^{mn \times mn} \quad (2)$$

with configuration matrix

$$\mathbf{X}^\top = [(\mathbf{X}^{(1)})^\top | (\mathbf{X}^{(2)})^\top | \dots | (\mathbf{X}^{(m)})^\top] \in \mathbb{R}^{mn \times d},$$

subject to $\mathbf{X}^{(i)} = \mathbf{G}\mathbf{W}^{(i)}$ for all $i \in [m]$. The “NA” entries in $\mathbf{\Delta}$ represent the reality that the dissimilarities across modalities are unknown a priori. This is accounted for in the objective function by zeroing out the contribution to the stress associated with these entries of $\tilde{\mathbf{\Delta}}$. the weight matrix \mathbf{W} is structured to zero out the missing data entries of η in the objective function $\sigma(\cdot)$. The constrained MDS iterative majorization algorithm of De Leeuw and Heiser (1980) can then be applied to approximately solve the 3-RSMDS model. As the JOFC procedure (see Algorithm 1) and the accelerated fJOFC procedure (see Algorithm 2) are both iterative majorization MDS procedures, we will provide the details of De Leeuw and Heiser (1980) applied to 3-RSMDS for the sake of comparison. The procedure of De Leeuw and Heiser (1980) consists of the following two iterated steps, given an initialization of the configuration $\mathbf{X}_{(0)}$:

1. At configuration $\mathbf{X}_{(t-1)}$, ignoring the constraint that $\mathbf{X}^{(i)} = \mathbf{G}\mathbf{W}^{(i)}$ for all $i \in [m]$, compute the unconstrained update $\tilde{\mathbf{X}}_{(t)}$ via the Guttman transform; see Borg and Groenen (2005).
2. Set $\mathbf{X}_{(t)} = \left[(\mathbf{X}_{(t)}^{(1)})^\top | (\mathbf{X}_{(t)}^{(2)})^\top | \dots | (\mathbf{X}_{(t)}^{(m)})^\top \right]$ to be the minimizer of

$$\text{trace}(\mathbf{X} - \tilde{\mathbf{X}}_{(t)})^\top \tilde{\mathbf{L}}(\mathbf{X} - \tilde{\mathbf{X}}_{(t)}),$$

over \mathbf{X} subject to the constraints $\mathbf{X}^{(i)} = \mathbf{G}\mathbf{W}^{(i)}$ for all $i \in \{1, 2, \dots, m\}$. Here, $\tilde{\mathbf{L}} \in \mathbb{R}^{mn \times mn}$ is the block diagonal matrix with $nI_n - J_n \in \mathbb{R}^{n \times n}$ in each of the m diagonal blocks, where $J_n = \mathbf{1}_n \mathbf{1}_n^\top \in \mathbb{R}^{n \times n}$, and $\mathbf{1}_n$ is the column vector of all one’s in \mathbb{R}^n . This minimization is often approached by alternating minimizing over \mathbf{G} for a fixed \mathbf{W} and then minimizing over \mathbf{W} for a fixed \mathbf{G} .

1.2.1 The JOFC framework

In the above 3-RSMDS framework, the matchedness of the n observations across the m dissimilarities is enforced via the $\mathbf{X}^{(i)} = \mathbf{G}\mathbf{W}^{(i)}$ constraints. In the JOFC algorithm, the matchedness constraint is built into the objective function as follows. Contrasting the

raw stress criterion in (1), the variant of JOFC we consider seeks to produce an unconstrained configuration $\mathbf{X}^\top = [(\mathbf{X}^{(1)})^\top | (\mathbf{X}^{(2)})^\top | \dots | (\mathbf{X}^{(m)})^\top] \in \mathbb{R}^{mn \times d}$, (where $(\mathbf{X}^{(i)})^\top = [(X_1^{(i)})^\top | (X_2^{(i)})^\top | \dots | (X_m^{(i)})^\top] \in \mathbb{R}^{n \times d}$, are the points associated with Δ_i) that minimizes the raw stress criterion

$$\sigma(\mathbf{X}) = \underbrace{\sum_{i=1}^m \sum_{1 \leq j < \ell \leq n} ([\Delta_i]_{j,\ell} - d_{j,\ell}(\mathbf{X}^{(i)}))^2}_{\text{fidelity}} + w \underbrace{\sum_{1 \leq i < j \leq m} \sum_{\ell=1}^n d(X_\ell^{(i)}, X_\ell^{(j)})^2}_{\text{commensurability}}, \quad (3)$$

where $d(\cdot, \cdot)$ is the Euclidean distance function. The raw stress criterion in JOFC is composed of three major pieces:

1. The ‘‘fidelity’’ term, $\sum_{i=1}^m \sum_{1 \leq j < \ell \leq n} ([\Delta_i]_{j,\ell} - d_{j,\ell}(\mathbf{X}^{(i)}))^2$, which measures the faithfulness of the embedding to the original dissimilarities, $\{\Delta_i\}_{i=1}^m$. Note the the fidelity is equal to the raw stress criterion in 3-RSMDS (1).
2. The ‘‘commensurability’’ term, $\sum_{1 \leq i < j \leq m} \sum_{\ell=1}^n d(X_\ell^{(i)}, X_\ell^{(j)})^2$, which measures how the geometry of the embeddings differs across modality. Similar to the role of the $\mathbf{X}^{(i)} = \mathbf{G}\mathbf{W}^{(i)}$ constraints in 3-RSMDS, in JOFC the commensurability term (softly) enforces the matchedness of the n data points across the m modalities. We also note that the commensurability is proportional to the objective function of three-way Procrustes analysis

$$\begin{aligned} \text{commensurability} &= \sum_{i < j}^m \text{trace}(\mathbf{X}^{(i)} - \mathbf{X}^{(j)})^\top (\mathbf{X}^{(i)} - \mathbf{X}^{(j)}) \\ &= m \sum_{i=1}^m \text{trace}(\mathbf{X}^{(i)} - \bar{\mathbf{X}})^\top (\mathbf{X}^{(i)} - \bar{\mathbf{X}}), \end{aligned} \quad (4)$$

where $\bar{\mathbf{X}} = m^{-1} \sum_{i=1}^m \mathbf{X}^{(i)}$.

3. The weighting of the fidelity versus the commensurability of the embedding provided by w . If $w \ll 1$, then the optimal embedding will preserve the within-modality dissimilarities at the expense of the cross-modality correspondence; i.e. each Δ_i will be fit separately. If $w \gg 1$, then the optimal embedding will preserve the cross-modality correspondence at the expense of the within-modality dissimilarities; i.e. from Eq (4) we see that $w \gg 1$ would force all of the $\mathbf{X}^{(i)}$ to be equal without concern for preserving the original Δ_i 's. In light of this, JOFC can be viewed as weakly constrained

Raw Stress MDS (see Borg and Groenen (2005) for detail), with w allowing us to continuously range between setting all $\mathbf{X}^{(i)}$'s to be equal but otherwise unconstrained ($w = \infty$) at one extreme versus embedding the Δ_i 's completely separately ($w = 0$) at the other.

The problem of choosing an optimal w was taken up in Adali and Priebe (2015). When the individual dissimilarities are normalized to have $\|\Delta_i\|_F = 1$ for all $i \in [m]$, the results of Adali and Priebe (2015) suggest that, under suitable model assumptions, the performance of the JOFC procedure is relatively robust to the choice of w . In application, a data-adaptive w could be chosen via the bootstrapping AUC-optimization testing procedure of Adali and Priebe (2015), although we do not pursue this further here.

As in 3-RSMDS, minimizing (3) can be seen as unconstrained Raw Stress MDS on the omnibus dissimilarity matrix

$$\mathbf{\Delta} = [\Delta_{i,j}] = \begin{bmatrix} \Delta_1 & \eta & \cdots & \eta \\ \eta & \Delta_2 & \cdots & \eta \\ \vdots & \vdots & \ddots & \vdots \\ \eta & \eta & \cdots & \Delta_m \end{bmatrix} \in \mathbb{R}^{mn \times mn}, \quad \eta = \begin{bmatrix} 0 & \text{NA} & \cdots & \text{NA} \\ \text{NA} & 0 & \cdots & \text{NA} \\ \vdots & \vdots & \ddots & \vdots \\ \text{NA} & \text{NA} & \cdots & 0 \end{bmatrix} \in \mathbb{R}^{n \times n}, \quad (5)$$

and configuration

$$\mathbf{X}^\top = [(\mathbf{X}^{(1)})^\top | (\mathbf{X}^{(2)})^\top | \cdots | (\mathbf{X}^{(m)})^\top] \in \mathbb{R}^{mn \times d},$$

with the associated weight matrix given by

$$\mathbf{W} = [W_{i,j}] = \begin{bmatrix} J_n - I_n & wI_n & \cdots & wI_n \\ wI_n & J_n - I_n & \cdots & wI_n \\ \vdots & \vdots & \ddots & \vdots \\ wI_n & wI_n \cdots & \cdots & J_n - I_n \end{bmatrix} \in \mathbb{R}^{mn \times mn}; \quad (6)$$

indeed, this is immediate as the raw stress criterion in (3) is equal to $\sigma(\mathbf{X}) = \sum_{i < j} W_{i,j} (\Delta_{i,j} - d_{i,j}(\mathbf{X}))^2$. Note that, as before, the weight matrix \mathbf{W} is structured to zero out the missing data entries of η in the objective function $\sigma(\cdot)$.

Note the different structure of Δ in JOFC versus $\tilde{\Delta}$ in 3-RSMDS. In JOFC, we impute the missing across modality dissimilarity between the same object to be 0, which allows us to build the matchedness constraint into the raw stress criterion (via the commensurability term). In both models, we treat inter-object, cross-modality dissimilarities as missing data, and this represents the assumption that these dissimilarities are often *not* available in the embedding procedure.

Remark 2. In Priebe et al. (2013), the missing cross-modality dissimilarity between modality i and modality j was imputed as $(\Delta_i + \Delta_j)/2$, and Δ was embedded using classical multidimensional scaling. Here we choose not to impute the missing data for two main reasons: imputing the cross-modality dissimilarities potentially increases the variance in our embedded points; and the special structure of \mathbf{W} in the missing data setting allows us to greatly speed up and parallelize the JOFC procedure (see Section 2). In addition, in many real data settings (see Section 4) the n objects originate from *disparate* data sources and are not simply repeated measurements of the same objects in a single space, which further complicates the very concept of cross-modality dissimilarities.

Similar to the approach in De Leeuw and Heiser (1980) for 3-RSMDS, our JOFC approach embeds Δ by minimizing (3) via successive Guttman transforms. As in the majorization algorithm for solving 3-RSMDS, the Guttman transform step of JOFC can be efficiently computed (see Algorithm 2). However, in JOFC the matchedness constraint is built into the raw stress criterion, and we are therefore able to avoid the potentially costly Step 2 of the 3-RSMDS procedure as outlined in Section 1.2. The JOFC algorithm proceeds as follows:

1. Initialize the configuration $\mathbf{X}_{(0)}$. One easily implemented initialization imputes the missing data entries of Δ as in Remark 2 and performs classical MDS on Δ ; see Step 1 of Algorithm 1 for detail.
2. For a given threshold $\epsilon > 0$, while $\sigma(\mathbf{X}_{(t)}) - \sigma(\mathbf{X}_{(t-1)}) > \epsilon$, iteratively update \mathbf{X}_{t-1} via the Guttman transform. To wit, let \mathbf{L} be the combinatorial Laplacian of the weight matrix \mathbf{W} (i.e., if \mathbf{D} is the diagonal matrix with $D_{i,i} = \sum_j W_{i,j}$, then $\mathbf{L} = \mathbf{D} - \mathbf{W}$),

and define

$$B(\mathbf{X})_{i,j} := \begin{cases} \frac{-W_{i,j}\Delta_{i,j}}{d_{i,j}(\mathbf{X})} & \text{if } i \neq j \text{ and } d_{i,j}(\mathbf{X}) \neq 0 \\ 0 & \text{if } i \neq j \text{ and } d_{i,j}(\mathbf{X}) = 0 \\ -\sum_{k=1, k \neq i}^n B(\mathbf{X})_{i,k} & \text{if } i = j. \end{cases} \quad (7)$$

Then the raw stress criterion (3) can be written

$$\sigma(\mathbf{X}_{(t)}) = \sum_{i < j} W_{i,j} \Delta_{i,j}^2 + \text{trace} \mathbf{X}_{(t)}^\top \mathbf{L} \mathbf{X}_{(t)} - 2 \text{trace} \mathbf{X}_{(t)}^\top B(\mathbf{X}_{(t)}) \mathbf{X}_{(t)},$$

which is majorized by

$$\sigma(\mathbf{X}_{(t)}) \leq \sum_{i < j} W_{i,j} \Delta_{i,j}^2 + \text{trace} \mathbf{X}_{(t)}^\top \mathbf{L} \mathbf{X}_{(t)} - 2 \text{trace} \mathbf{X}_{(t)}^\top B(\mathbf{X}_{(t-1)}) \mathbf{X}_{(t-1)}, \quad (8)$$

a quadratic function of $\mathbf{X}_{(t)}$. The minimizer of (8) can be found by solving the stationary equation $\nabla \sigma(\mathbf{X}_{(t)}) = 2\mathbf{L}\mathbf{X}_{(t)} - 2B(\mathbf{X}_{(t-1)})\mathbf{X}_{(t-1)} = 0$. The Guttman transform updates a configuration $\mathbf{X}_{(t-1)}$ by solving $\mathbf{L}\mathbf{X}_{(t)} = B(\mathbf{X}_{(t-1)})\mathbf{X}_{(t-1)}$; in the multidimensional scaling literature, this transformation is often written as $\mathbf{X}_{(t)} = \Gamma(\mathbf{X}_{(t-1)}) = \mathbf{L}^\dagger B(\mathbf{X}_{(t-1)})\mathbf{X}_{(t-1)}$ where \mathbf{L}^\dagger is the Moore-Penrose pseudoinverse of \mathbf{L} . Notice that $\mathbf{X}_{(t)}$ is centered at zero even if $\mathbf{X}_{(t-1)}$ is not centered at zero.

For JOFC, the resulting iterative algorithm is summarized in Algorithm 1. Note that the sequence of steps generated by successive Guttman transforms is derived via majorization, and we note that Algorithm 1 is closely related to the popular SMACOF algorithm for metric multidimensional scaling; see De Leeuw and Heiser (1980); de Leeuw (1988).

Remark 3. In all of the experiments in Section 4, the threshold ϵ is set to $10^{-6} \binom{nm}{2}$; i.e., we terminate the procedure when the normalized stress $\sigma_N(\cdot) := \sigma(\cdot) / \binom{nm}{2}$ fails to decrease by at least 10^{-6} between successive iterations. Note however that, in practice, the sequential Guttman transforms often exhibit good global properties, and only a few iterations are required to obtain a sufficiently good suboptimal embedding, see Kearsley et al. (1995). We empirically observe this phenomena in Figure 2, where we see that the configuration obtained by fJOFC can stabilize after only relatively few iterates.

Algorithm 1 JOFC Algorithm for Manifold Matching (see Section 1.2.1 for detail)

Require: Omnibus dissimilarity matrix Δ , weight matrix \mathbf{W} , embedding dimension d ,
 $\text{tol} = \epsilon$

Ensure: $\mathbf{X} \in \mathbb{R}^{mn \times d}$, a configuration of points in \mathbb{R}^d

- 1: Initialize $\mathbf{X}_{(0)}$ via cMDS (classical MDS, see Torgerson (1952); Borg and Groenen (2005) for detail) of Δ
 - i. Set $\Delta^{(2)}$ to be the element-wise square of Δ ; i.e., $\Delta_{i,j}^{(2)} = (\Delta_{i,j})^2$;
 - ii. Compute $\mathbf{P} = -\frac{1}{2}(I_{mn} - \frac{1}{mn}J_{mn})\Delta^{(2)}(I_{mn} - \frac{1}{mn}J_{mn})$;
 - iii. Compute the d largest eigenvalues $\lambda_1, \lambda_2, \dots, \lambda_d$ of \mathbf{P} with corresponding eigenvectors u_1, u_2, \dots, u_d ;
 - iv. Set $\mathbf{X}_{(0)} = [u_1|u_2|\dots|u_d]\text{diag}(\lambda_i)^{1/2}$;
 - 2: Compute $\sigma(\mathbf{X}_{(0)})$
 - 3: **while** $\sigma(\mathbf{X}_{(t)}) - \sigma(\mathbf{X}_{(t-1)}) > \epsilon$ **do**
 - 4: $\mathbf{X}_{(t)} = \mathbf{L}^\dagger B(\mathbf{X}_{(t-1)})\mathbf{X}_{(t-1)}$
 - 5: Compute $\sigma(\mathbf{X}_{(t)})$
 - 6: **end while**
 - 7: Output the final iteration $\mathbf{X}_{(\text{final})}$
-

In general, \mathbf{L}^\dagger must be calculated by singular value or QR decomposition, which may be prohibitively expensive if mn is large, with computational complexity of order $O(m^3n^3)$. Fortunately, there are many applications in which the special structure of the weight matrix \mathbf{W} allows for direct calculation of \mathbf{L}^\dagger , sometimes with subsequent simplification of $\mathbf{L}^\dagger B(\mathbf{X}_{(t-1)})\mathbf{X}_{(t-1)}$. Examples include the familiar case of unit weights (which is the case for the Guttman transform needed in Step 1 of the 3-RSMDS algorithm in Section 1.2) and the case of symmetric block-circulant matrices, see Gower and Groenen (1990); Gower (2006). In Section 2, we demonstrate that the special structure of JOFC also permits the direct calculation of \mathbf{L}^\dagger which then results in a much simplified calculation of $\mathbf{L}^\dagger B(\mathbf{X}_{(t-1)})\mathbf{X}_{(t-1)}$.

2 Fast JOFC

In each iteration of the JOFC algorithm (Algorithm 1), we update the configuration via a Guttman transform $\mathbf{X}_{(t)} = \mathbf{L}^\dagger B(\mathbf{X}_{(t-1)})\mathbf{X}_{(t-1)}$. Computationally, this involves

1. A single calculation of \mathbf{L}^\dagger , which naively has algorithmic complexity $O((mn)^3)$ given an SVD (or QR decomposition) based pseudoinverse algorithm. Clearly, as \mathbf{L}^\dagger does not vary in t , we do not need to recalculate this pseudoinverse in every iteration.
2. Computing $\mathbf{L}^\dagger B(\mathbf{X}_{(t-1)})\mathbf{X}_{(t-1)}$, which has complexity $O((mn)^2d)$.

Therefore, given a bounded number of iterations and assuming $d < mn$, the JOFC algorithm has algorithmic complexity $O((mn)^3)$.

To speed up the JOFC procedure, we first note that the form of the JOFC weight matrix allows us to algebraically compute \mathbf{L}^\dagger . Next, we show that the resulting form of the pseudoinverse allows us to greatly simplify the computation of $\mathbf{L}^\dagger B(\mathbf{X}_{(t-1)})\mathbf{X}_{(t-1)}$. In addition, the computation of $\mathbf{L}^\dagger B(\mathbf{X}_{(t-1)})\mathbf{X}_{(t-1)}$ easily lends itself to parallelization.

2.1 Computing \mathbf{L}^\dagger

The first step in speeding up Algorithm 1 is algebraically computing the pseudoinverse \mathbf{L}^\dagger . Here, we present the computation of \mathbf{L}^\dagger in the case of a more general weight matrix than considered in Eq. (6); namely, we will consider here \mathbf{W} of the form

$$\mathbf{W} = [W_{i,j}] = \begin{bmatrix} w_{1,1}(J_n - I_n) & w_{1,2}I_n & \cdots & w_{1,m}I_n \\ w_{2,1}I_n & w_{2,2}(J_n - I_n) & \cdots & w_{2,m}I_n \\ \vdots & \vdots & \ddots & \vdots \\ w_{m,1}I_n & w_{m,2}I_n \cdots & \cdots & w_{m,m}(J_n - I_n) \end{bmatrix} \in (\mathbb{R}^+)^{mn \times mn}; \quad (9)$$

with $w_{i,j} = w_{j,i}$ for all $i, j \in [m]$ such that $i \neq j$. This form of \mathbf{W} allows for different weightings across and within modalities. The case of equal weights off diagonal, i.e., the \mathbf{W} in Eq. (6), will then be realized as a special case of this more general \mathbf{W} .

In Appendix A, we prove the following. Writing

$$\mathcal{W} = \begin{bmatrix} nw_{1,1} + \sum_{j \neq 1} w_{1,j} & -w_{1,2} & \cdots & -w_{1,m} \\ -w_{2,1} & nw_{2,2} + \sum_{j \neq 2} w_{2,j} & \cdots & -w_{2,m} \\ \vdots & \vdots & \ddots & \vdots \\ -w_{m,1} & -w_{m,2} \cdots & \cdots & nw_{m,m} + \sum_{j \neq m} w_{m,j} \end{bmatrix}, \quad (10)$$

and $\text{diag}(w_{i,i}) := \text{diag}(w_{1,1}, w_{2,2}, \dots, w_{m,m})$, we algebraically compute \mathbf{L}^\dagger via

$$\mathbf{L}^\dagger = \mathcal{W}^{-1} \otimes I_n + \left[- \left(\mathcal{W} + n \left(\frac{J_m}{mn} - \text{diag}(w_{i,i}) \right) \right)^{-1} \left(\frac{J_m}{mn} - \text{diag}(w_{i,i}) \right) \mathcal{W}^{-1} - \frac{J_m}{mn} \right] \otimes J_n.$$

While brute force computation of \mathcal{W}^{-1} (and \mathcal{Z}) would incur a $O(m^3)$ cost as opposed to the $O(m^3n^3)$ cost of a brute force computation of \mathbf{L}^\dagger , structured weight matrices can greatly simplify this computation. For example, if \mathbf{W} is of the form of Eq. (6), then a brief calculation yields that

$$\mathcal{W}^{-1} = \begin{bmatrix} \frac{n+w}{n(n+mw)} & \frac{w}{n(n+mw)} & \cdots & \frac{w}{n(n+mw)} \\ \frac{w}{n(n+mw)} & \frac{n+w}{n(n+mw)} & \cdots & \frac{w}{n(n+mw)} \\ \vdots & \vdots & \ddots & \vdots \\ \frac{w}{n(n+mw)} & \frac{w}{n(n+mw)} \cdots & \cdots & \frac{n+w}{n(n+mw)} \end{bmatrix} \in \mathbb{R}^{m \times m}, \quad (11)$$

and

$$\begin{aligned} & - \left(\mathcal{W} + n \left(\frac{J_m}{mn} - \text{diag}(w_{i,i}) \right) \right)^{-1} \left(\frac{J_m}{mn} - \text{diag}(w_{i,i}) \right) \mathcal{W}^{-1} - \frac{J_m}{mn} \\ &= \begin{bmatrix} \frac{-m^2w^2+mn^2-mnw-n^2}{wn^2m^2(n+wm)} & \frac{-m^2w^2-mnw-n^2}{wn^2m^2(n+wm)} & \cdots & \frac{-m^2w^2-mnw-n^2}{wn^2m^2(n+wm)} \\ \frac{-m^2w^2-mnw-n^2}{wn^2m^2(n+wm)} & \frac{-m^2w^2+mn^2-mnw-n^2}{wn^2m^2(n+wm)} & \cdots & \frac{-m^2w^2-mnw-n^2}{wn^2m^2(n+wm)} \\ \vdots & \vdots & \ddots & \vdots \\ \frac{-m^2w^2-mnw-n^2}{wn^2m^2(n+wm)} & \frac{-m^2w^2-mnw-n^2}{wn^2m^2(n+wm)} \cdots & \cdots & \frac{-m^2w^2+mn^2-mnw-n^2}{wn^2m^2(n+wm)} \end{bmatrix} \in \mathbb{R}^{m \times m}. \end{aligned}$$

We shall see in Section 2.2 how these algebraic computations greatly speed-up the computation of the Guttman transform in the fJOFC procedure.

Also note that in implementing the fJOFC algorithm, only \mathcal{W}^{-1} needs to be computed. Indeed, $\mathbf{1}_{mn}^\top B(\mathbf{X}_{(t-1)}) = B(\mathbf{X}_{(t-1)})\mathbf{1}_{mn} = 0$, which immediately implies that

$$\left(\left[- \left(\mathcal{W} + n \left(\frac{J_m}{mn} - \text{diag}(w_{i,i}) \right) \right)^{-1} \left(\frac{J_m}{mn} - \text{diag}(w_{i,i}) \right) \mathcal{W}^{-1} - \frac{J_m}{mn} \right] \otimes J_n \right) B(\mathbf{X}_{(t-1)}) = \mathbf{0}_{mn}.$$

Resultingly, the Gutman transform in the t -th iteration of fJOFC is computed simply as

$$\mathbf{X}_{(t)} = (\mathcal{W}^{-1} \otimes I_n) B(\mathbf{X}_{(t-1)})\mathbf{X}_{(t-1)}.$$

Remark 4. The key to computing the form of \mathbf{L}^\dagger is realizing that \mathbf{L}^\dagger can be written as

$$\mathbf{L}^\dagger = \left(\mathbf{L} + \frac{1}{mn} J_{mn} \right)^{-1} - \frac{1}{mn} J_{mn}.$$

We then compute the exact form of $(\mathbf{L} + \frac{1}{mn} J_{mn})^{-1}$ by inverting the structured matrix

$$\mathbf{L} + \frac{1}{mn} J_{mn} = \mathcal{W} \otimes I_n + \left(\frac{1}{mn} J_m - \text{diag}(w_{i,i}) \right) \otimes J_n.$$

This inverse computation (Theorem 10 in Appendix A) can be generalized to the following Woodbury-type (Woodbury, 1950) matrix identity for the sum of Kronecker products. Let $A, B \in \mathbb{R}^{m \times m}$ be matrices such that A and $(A + nB)$ are invertible matrices. Then it follows that

$$(A \otimes I_n + B \otimes J_n)^{-1} = A^{-1} \otimes I_n - (A + nB)^{-1} B A^{-1} \otimes J_n.$$

This formula generalizes Theorem 10, and we are presently exploring different use cases for such an identity.

Remark 5. Even given identical initializations, the fJOFC algorithm (Algorithm 2), and the JOFC algorithm may not give identical embeddings of Δ , as JOFC relies on a computational approximation of \mathbf{L}^\dagger , while fJOFC exactly algebraically computes \mathbf{L}^\dagger .

2.1.1 More general weight matrices

We described above how the structured \mathbf{W} of Eq. (6) offers an easily computed form for \mathcal{W}^{-1} , and here we will briefly outline some other potentially useful structured weight matrices that lend themselves to easily compute \mathcal{W}^{-1} . If \mathbf{W} is of the form

$$\mathbf{W} = [W_{i,j}] = \begin{bmatrix} w_{1,1}(J_n - I_n) & w_{1,1}w_{2,2}I_n & \cdots & w_{1,1}w_{m,m}I_n \\ w_{1,1}w_{2,2}I_n & w_{2,2}(J_n - I_n) & \cdots & w_{2,2}w_{m,m}I_n \\ \vdots & \vdots & \ddots & \vdots \\ w_{1,1}w_{m,m}I_n & w_{2,2}w_{m,m}I_n \cdots & \cdots & w_{m,m}(J_n - I_n) \end{bmatrix} \in (\mathbb{R}^+)^{mn \times mn}; \quad (12)$$

so that each modality has its own (potentially unique) weight, and the cross modality dissimilarities are weighted via a product of the within modality weights, then

$$\mathcal{W}^{-1} = \frac{\text{diag}(w_{i,i})^{-1}}{n + \sum_i w_{i,i}} + \frac{1}{n(n + \sum_i w_{i,i})} J_m,$$

so that the k, ℓ -th entry of \mathcal{W}^{-1} is equal to

$$\mathcal{W}_{k,\ell}^{-1} = \begin{cases} \frac{1}{w_{k,k}(n + \sum_i w_{i,i})} + \frac{1}{n(n + \sum_i w_{i,i})} & \text{if } k = \ell \\ \frac{1}{n(n + \sum_i w_{i,i})} & \text{else.} \end{cases}$$

Increasing the weight of the within-modality embeddings can easily be achieved by letting \mathcal{W} be set to

$$\mathcal{W} = cn \cdot \text{diag}(w_{i,i}) + \text{diag}(w_{i,i}) \left(\left(\sum_i w_{i,i} \right) I_m - J_m \text{diag}(w_{i,i}) \right),$$

in which case

$$\mathcal{W}^{-1} = \frac{\text{diag}(w_{i,i})^{-1}}{cn + \sum_i w_{i,i}} + \frac{1}{cn(cn + \sum_i w_{i,i})} J_m.$$

Increasing (resp., decreasing) the value of the constant c will have the effect of emphasizing (resp., deemphasizing) the fidelity of the subsequent embedding.

2.2 Effect on the computation of $\mathbf{L}^\dagger B(\mathbf{X}_{(t-1)})\mathbf{X}_{(t-1)}$

Exploiting the form of \mathbf{L}^\dagger computed above, we use the special structure of $B(\mathbf{X}_{(t-1)})$ to simplify and speed up the calculation of the Guttman transform needed in the t -th iteration of the JOFC algorithm.

We first note that $B(\mathbf{X}_{(t-1)})$ is block diagonal, with m diagonal blocks each of size $n \times n$. We will denote the diagonal blocks of $B(\mathbf{X}_{(t-1)})$ by B_1, B_2, \dots, B_m . By construction,

$$\mathbf{1}_{mn}^\top B(\mathbf{X}_{(t-1)}) = B(\mathbf{X}_{(t-1)})\mathbf{1}_{mn} = 0,$$

and therefore $\mathbf{1}_n^\top B_j = B_j\mathbf{1}_n = 0$ for all $j = 1, 2, \dots, m$. It follows that $B_j J_n = J_n B_j = 0$ for all $j = 1, 2, \dots, m$. Defining

$$A' := \frac{n+w}{n(n+mw)} I_n, \text{ and } C' := \frac{w}{n(n+mw)} I_n,$$

we arrive at

$$\mathbf{L}^\dagger B(\mathbf{X}_{(t-1)}) = \begin{bmatrix} A' & C' & \cdots & C' \\ C' & A' & \cdots & C' \\ \vdots & \vdots & \ddots & \vdots \\ C' & C' & \cdots & A' \end{bmatrix} \begin{bmatrix} B_1 & 0 & \cdots & 0 \\ 0 & B_2 & \cdots & 0 \\ \vdots & \vdots & \ddots & \vdots \\ 0 & 0 & \cdots & B_m \end{bmatrix},$$

and so

$$\begin{aligned} \mathbf{X}_{(t)} &= \mathbf{L}^\dagger B(\mathbf{X}_{(t-1)})\mathbf{X}_{(t-1)} = \begin{bmatrix} A' & C' & \cdots & C' \\ C' & A' & \cdots & C' \\ \vdots & \vdots & \ddots & \vdots \\ C' & C' & \cdots & A' \end{bmatrix} \begin{bmatrix} B_1 & 0 & \cdots & 0 \\ 0 & B_2 & \cdots & 0 \\ \vdots & \vdots & \ddots & \vdots \\ 0 & 0 & \cdots & B_m \end{bmatrix} \begin{bmatrix} \mathbf{X}_{(t-1)}^{(1)} \\ \mathbf{X}_{(t-1)}^{(2)} \\ \vdots \\ \mathbf{X}_{(t-1)}^{(m)} \end{bmatrix} \\ &= \left(\frac{n}{n(n+mw)} I_{nm} + \frac{w}{n(n+mw)} \begin{bmatrix} I_n & I_n & \cdots & I_n \\ I_n & I_n & \cdots & I_n \\ \vdots & \vdots & \ddots & \vdots \\ I_n & I_n & \cdots & I_n \end{bmatrix} \right) \begin{bmatrix} B_1 \mathbf{X}_{(t-1)}^{(1)} \\ B_2 \mathbf{X}_{(t-1)}^{(2)} \\ \vdots \\ B_m \mathbf{X}_{(t-1)}^{(m)} \end{bmatrix}. \end{aligned} \quad (13)$$

From (13), it is immediate that the update is realized via

$$\mathbf{X}_{(t)}^{(j)} = \frac{n}{n(n+mw)} B_j \mathbf{X}_{(t-1)}^{(j)} + \sum_{\ell=1}^m \frac{w}{n(n+mw)} B_\ell \mathbf{X}_{(t-1)}^{(\ell)}. \quad (14)$$

Remark 6. Note that to efficiently compute (14), we can first compute each $B_\ell \mathbf{X}_{(t-1)}^{(\ell)}$ in parallel for $\ell \in [m]$, and then compute the update in Eq. (14).

2.3 The fJOFC algorithm

The algebraic computation of \mathbf{L}^\dagger in Section 2.1 combined with the computation of the Guttman transform of Section 2.2 combine to give us the fJOFC algorithm, which is detailed below and in Algorithm 2.

The fJOFC algorithm proceeds as follows:

1. Initialize the configuration $\mathbf{X}_{(0)}$. If the initialization of the JOFC procedure in Remark 2 is too computationally intensive (in particular, the initialization uses cMDS to embed the $mn \times mn$ omnibus dissimilarity with off-diagonal blocks imputed to be $(\Delta_i + \Delta_j)/2$) we could proceed as follows: first, use cMDS to embed the average

Algorithm 2 fJOFC: Fast JOFC Algorithm for Manifold Matching

Require: Omnibus dissimilarity matrix Δ , weight matrix \mathbf{W} , embedding dimension d ,
tol = ϵ

Ensure: $\mathbf{X} \in \mathbb{R}^{mn \times d}$, a configuration of points in \mathbb{R}^d

- 1: Set ξ_0 to be the configuration obtained via cMDS of $(\sum_i \Delta_i) / m$ (see Step 1. of Algorithm 1 for detail); Center ξ_0 via $\xi_0 = \xi_0(I_n - \frac{1}{n}J_n)$;
 - 2: **for** $i=1,2,\dots,m$ **do**
 - 3: Set ξ_i to be the configuration obtained via cMDS of Δ_i ; ; Center ξ_i via $\xi_i = \xi_i(I_n - \frac{1}{n}J_n)$;
 - 4: Set $\mathbf{X}_{(0)}^{(i)}$ to be the orthogonal Procrustes fit of ξ_i onto ξ_0 ;
 - i. Set $T = \xi_0^T \xi_i$;
 - ii. Let $U\Sigma V^T$ be the singular value decomposition of T ;
 - iii. Set $\mathbf{X}_{(0)}^{(i)} = \xi_i U V^T$
 - 5: **end for**
 - 6: Set $\mathbf{X}_{(0)}^\top = \left[(\mathbf{X}_{(0)}^{(1)})^\top \mid (\mathbf{X}_{(0)}^{(2)})^\top \mid \dots \mid (\mathbf{X}_{(0)}^{(m)})^\top \right]$
 - 7: Compute $\sigma(\mathbf{X}_{(0)})$ as in Remark 7
 - 8: **while** $\sigma(\mathbf{X}_{(t)}) - \sigma(\mathbf{X}_{(t-1)}) > \epsilon$ **do**
 - 9: **for** $j=1,2,\dots,m$ **do**
 - 10: Compute $B(\mathbf{X}_{(t-1)}^{(j)})\mathbf{X}_{(t-1)}^{(j)}$
 - 11: **end for**
 - 12: **for** $j=1,2,\dots,m$ **do**
 - 13: Set $\mathbf{X}_{(t)}^{(j)} = \frac{n}{n(n+nw)}B(\mathbf{X}_{(t-1)}^{(j)})\mathbf{X}_{(t-1)}^{(j)} + \sum_{\ell=1}^m \frac{w}{n(n+nw)}B(\mathbf{X}_{(t-1)}^{(\ell)})\mathbf{X}_{(t-1)}^{(\ell)}$
 - 14: **end for**
 - 15: Set $\mathbf{X}_{(t)}^\top = \left[(\mathbf{X}_{(t)}^{(1)})^\top \mid (\mathbf{X}_{(t)}^{(2)})^\top \mid \dots \mid (\mathbf{X}_{(t)}^{(m)})^\top \right]$
 - 16: Compute $\sigma(\mathbf{X}_{(t)})$ as in Remark 7
 - 17: **end while**
 - 18: Output the final iteration $\mathbf{X}_{(\text{final})}$
-

dissimilarity matrix $(\sum_i \Delta_i) / m$, obtaining the configuration ξ_0 ; use cMDS to embed each Δ_i and set $\mathbf{X}_{(0)}^{(i)}$ to be the orthogonal Procrustes fit of the embedding to ξ_0 —see Step 4 of Algorithm 2 for detail.

2. Given current configuration $\mathbf{X}_{(t-1)}$ and error threshold ϵ , while $\sigma(\mathbf{X}_{(t)}) - \sigma(\mathbf{X}_{(t-1)}) > \epsilon$, compute the Guttman transform of $\mathbf{X}_{(t-1)}$ to obtain $\mathbf{X}_{(t)}$ as outlined in Section 2.2 (lines 9-15 of Algorithm 2). To wit, first compute each $B(\mathbf{X}_{(t-1)}^{(j)})\mathbf{X}_{(t-1)}^{(j)}$. The update is then realized by setting

$$\mathbf{X}_{(t)}^{(j)} = \frac{n}{n(n+nw)} B(\mathbf{X}_{(t-1)}^{(j)})\mathbf{X}_{(t-1)}^{(j)} + \sum_{\ell=1}^m \frac{w}{n(n+nw)} B(\mathbf{X}_{(t-1)}^{(\ell)})\mathbf{X}_{(t-1)}^{(\ell)}$$

for all $j \in [m]$. Each of these m updates has computational complexity $O(mn^2d)$.

Remark 7. Further speeding up the fJOFC procedure, from Eq. (3), we see that to compute $\sigma(\mathbf{X})$, we need not compute all $\binom{mn}{2}$ pairwise distance between rows of \mathbf{X} . Indeed, we only need to compute $m\binom{n}{2} + \binom{m}{2}n$ interpoint distances. Indeed, the fidelity can be written as

$$\sum_{i=1}^m \sum_{1 \leq j < \ell \leq n} ([\Delta_i]_{j,\ell} - d_{j,\ell}(\mathbf{X}^{(i)}))^2 = \frac{1}{2} \sum_{i=1}^m \|\Delta_i - d(\mathbf{X}^{(i)})\|_F^2,$$

and the commensurability requires $\binom{m}{2}$ paired distance calculations amongst the n points across the m modalities.

Given a bounded number of Guttman transform updates, the fJOFC algorithm has complexity $O(m^2n^2d)$. Contrasting this with the $O((mn)^3)$ complexity of JOFC points to the dramatic speedup achieved by fJOFC; see Section 4 for further empirical demonstrations of this computational savings. We also recall that, even with identical initializations, the JOFC iterates and fJOFC iterates will not agree in general. The JOFC iterates rely on an approximate computation of \mathbf{L}^\dagger while the fJOFC iterates utilize an exact algebraically computed \mathbf{L}^\dagger . Hence, the fJOFC iterates are not only more efficiently computed than the corresponding JOFC iterates, they are also less noisy.

Remark 8. Each step of the fJOFC procedure easily lends itself to parallel computation. Implemented in parallel, given a bounded number of Guttman transform updates, fJOFC has complexity $O(m^2n^2d/c)$ when run in parallel over c cores.

3 Fast out-of-sample embedding for JOFC

The out-of-sample embedding framework was developed for classical MDS in Trosset and Priebe (2008) and for Raw Stress MDS in Ma (2010). Extending the latter, we develop

the out-of-sample embedding framework for JOFC. We then demonstrate how this out-of-sample embedding can be dramatically sped-up by exploiting the special structure of the associated JOFC weight matrix, akin to the speedup of fJOFC over JOFC, and empirically demonstrate the efficiency of the procedure in Section 4.4.

Given a configuration $\mathbf{X} \in \mathbb{R}^{mn \times d}$ obtained via JOFC (or fJOFC) applied to $\Delta \in \mathbb{R}^{mn \times mn}$, we observe a new object \mathcal{O} , giving rise to the out-of-sample omnibus dissimilarity

$$\Delta^{(o)} = [\Delta_{i,j}^{(o)}] = \begin{bmatrix} \Delta_1^{(o)} & \eta & \cdots & \eta \\ \eta & \Delta_2^{(o)} & \cdots & \eta \\ \vdots & \vdots & \ddots & \vdots \\ \eta & \eta & \cdots & \Delta_m^{(o)} \end{bmatrix} \in \mathbb{R}^{m(n+1) \times m(n+1)}; \Delta_i^{(o)} = \begin{bmatrix} \Delta_i & \delta_i \\ \delta_i^\top & 0 \end{bmatrix} \in \mathbb{R}^{n+1 \times n+1},$$

where, for each $i \in [m]$, δ_i represents the within modality dissimilarities between \mathcal{O} and the in sample-data objects for the i -th modality.

While we could run JOFC (or fJOFC) on the full $\Delta^{(o)}$, if m or n is large this often becomes computationally burdensome. Rather, without re-embedding Δ , we seek to embed \mathcal{O} into the configuration space determined by \mathbf{X} so as to best preserve both the matchedness across the m versions of \mathcal{O} and the within modality dissimilarities provided by $\{\delta_i\}_{i=1}^m$. In the JOFC Raw Stress framework, the out-of-sample raw stress criterion is given by

$$\sigma_{\mathbf{X}}(\mathbf{y}) = \underbrace{\sum_{i=1}^m \sum_j (\delta_i(j) - d(\mathbf{X}_j^{(i)}, \mathbf{y}_j))^2}_{\text{out-of-sample fidelity}} + w \underbrace{\sum_{i < j} d(\mathbf{y}_i, \mathbf{y}_j)^2}_{\text{out-of-sample commensurability}}, \quad (15)$$

where $\mathbf{y}^\top = [\mathbf{y}_1^\top | \mathbf{y}_2^\top | \cdots | \mathbf{y}_m^\top] \in \mathbb{R}^{m \times d}$ is the configuration obtained for the new out-of-sample observation \mathcal{O} .

Reordering the rows and columns of $\Delta^{(o)}$ slightly,

$$\Delta^{(o)} = \begin{bmatrix} & & & & \delta_1 & NA & \cdots & NA \\ & & & & NA & \delta_2 & \cdots & NA \\ & & \Delta & & \vdots & \vdots & \ddots & \vdots \\ & & & & NA & NA & \cdots & \delta_m \\ \delta_1^\top & NA & \cdots & NA & 0 & 0 & \cdots & 0 \\ NA & \delta_2^\top & \cdots & NA & 0 & 0 & \cdots & 0 \\ \vdots & \vdots & \ddots & \vdots & \vdots & \vdots & \ddots & \vdots \\ NA & NA & \cdots & \delta_m^\top & 0 & 0 & \cdots & 0 \end{bmatrix},$$

we see that the raw stress criterion (15) can be written as

$$\sigma_{\mathbf{X}}(\mathbf{y}) = \sum_{i < j} \mathbf{W}_{i,j}^{(o)} (\Delta_{i,j}^{(o)} - d_{i,j}(\mathbf{X}^{(o)}))^2,$$

with the weight matrix $\mathbf{W}^{(o)}$ and configuration $\mathbf{X}^{(o)}$ given by (where for $h, k \in \mathbb{Z} > 0$, $\mathbf{0}_{h,k}$ is the $h \times k$ matrix of all 0's)

$$\mathbf{W}^{(o)} = \begin{bmatrix} \mathbf{0}_{mn,mn} & I_m \otimes \mathbf{1}_n \\ I_m \otimes \mathbf{1}_n^\top & wJ_{m,m} - wI_m \end{bmatrix}, \quad \mathbf{X}^{(o)} = \begin{bmatrix} \mathbf{X} \\ \mathbf{y}_1 \\ \mathbf{y}_2 \\ \vdots \\ \mathbf{y}_m \end{bmatrix}.$$

Decompose the Laplacian of $\mathbf{W}^{(o)}$ via

$$\mathbf{L}^{(o)} = \begin{matrix} & mn \text{ cols} & m \text{ cols} \\ mn \text{ rows} & \begin{pmatrix} L_{1,1} & L_{1,2} \\ L_{1,2}^\top & L_{2,2} \end{pmatrix} \\ m \text{ rows} & \end{matrix},$$

and define $B(\mathbf{X}^{(o)})$ as in Eq. (7), a similar decomposition of B is given by

$$B(\mathbf{X}^{(o)}) = \begin{matrix} & mn \text{ cols} & m \text{ cols} \\ mn \text{ rows} & \begin{pmatrix} B_{1,1} & B_{1,2} \\ B_{1,2}^\top & B_{2,2} \end{pmatrix} \\ m \text{ rows} & \end{matrix} = \begin{bmatrix} B_{1,1} & & & B_{1,2} \\ & \text{diag} \left(\mathbf{1}^T \left(\delta_i \circ \frac{1}{d(\mathbf{X}^{(i)}, \mathbf{y}^{(t-1)})} \right) \right) & & \\ & & & \end{bmatrix},$$

where “ \circ ” is the Hadamard product, and for each $j \in [m]$,

$$\frac{1}{d(\mathbf{X}^{(j)}, \mathbf{y}_{(t-1)})} = \left(\frac{1}{d(\mathbf{X}_1^{(j)}, (\mathbf{y}_{(t-1)})_1)}, \dots, \frac{1}{d(\mathbf{X}_m^{(j)}, (\mathbf{y}_{(t-1)})_m)} \right)^\top.$$

Note that

$$B_{1,2} = - \begin{bmatrix} \delta_1 \circ \frac{1}{d(\mathbf{X}^{(1)}, \mathbf{y}_{(t-1)})} & \mathbf{0}_m & \cdots & \mathbf{0}_m \\ \mathbf{0}_m & \delta_2 \circ \frac{1}{d(\mathbf{X}^{(2)}, \mathbf{y}_{(t-1)})} & \cdots & \mathbf{0}_m \\ \vdots & \vdots & \ddots & \vdots \\ \mathbf{0}_m & \mathbf{0}_m & \cdots & \delta_m \circ \frac{1}{d(\mathbf{X}^{(m)}, \mathbf{y}_{(t-1)})} \end{bmatrix}.$$

A similar majorization argument to that of in-sample JOFC yields the out-of-sample embedding procedure:

1. Initialize the out-of-sample configuration at a random initialization $\mathbf{y} = \mathbf{y}_{(0)}$.
2. While $\sigma_{\mathbf{X}}(\mathbf{y}_{(t)}) - \sigma_{\mathbf{X}}(\mathbf{y}_{(t-1)}) > \epsilon$ for a predetermined threshold ϵ , update $\mathbf{y}_{(t)}$ via the Guttman transform:

$$\mathbf{y}_{(t)} = L_{2,2}^\dagger (B_{1,2}^\top - L_{1,2}^\top) \mathbf{X} + L_{2,2}^\dagger \cdot \text{diag} \left(\mathbf{1}^T \left(\delta_i \circ \frac{1}{d(\mathbf{X}^{(i)}, \mathbf{y}_{(t-1)})} \right) \right) \mathbf{y}_{(t-1)}. \quad (16)$$

Derivation of this update via majorization is completely analogous to the derivation of the JOFC update step, and so details are suppressed.

As $L_{2,2} = (n + mw)I_m - wJ_m$, it is immediate that $L_{2,2}^\dagger = \frac{1}{n+mw}I_m + \frac{w}{n(n+mw)}J_m$. Therefore, to efficiently compute (16), we:

1. For each $j \in [m]$, compute

$$\xi_j := \left(-\delta_j \circ \frac{1}{d(\mathbf{X}^{(j)}, \mathbf{y}_{(t-1)})} + \mathbf{1}_n \right)^\top \mathbf{X}^{(j)},$$

and

$$\psi_j := \mathbf{1}^T \left(\delta_i \circ \frac{1}{d(\mathbf{X}^{(i)}, \mathbf{y}_{(t-1)})} \right).$$

For each $j \in [m]$, this vector-matrix multiplication has complexity $O(nd)$, and the full complexity of this step is $O(nmd)$.

2. Routine computations then yield the following simplification of the Guttman transform update:

$$\begin{aligned}
 (\mathbf{y}^{(t)})_j &= \frac{\xi_j}{n + mw} + \frac{w}{n(n + mw)} \sum_{k=1}^m \xi_k \\
 &\quad + \frac{\psi_j}{n + mw} (\mathbf{y}^{(t-1)})_j + \frac{w}{n(n + mw)} \sum_{k=1}^m \psi_k \cdot (\mathbf{y}^{(t-1)})_k
 \end{aligned}$$

each of which has complexity $O(d)$, and the full complexity of this step is $O(md)$

Given a fixed number of modalities m and a bounded number of iterates in the algorithm, the complexity of embedding each new out-of-sample observation is linear in n , allowing for this out-of-sample procedure to be efficiently implemented on very large data sets. We note that the details for simultaneously embedding $k > 1$ out-of-sample points are completely analogous to the $k = 1$ case and so are omitted.

4 Results

In this section we both compare and contrast fJOFC and 3-RSMDS and demonstrate the dramatic run time increase achievable by fJOFC versus JOFC over a variety of real and simulated data examples; note that all run times are measured in seconds. In all examples, the algorithms were implemented on a MacBook Pro with a 2.6 GHz Intel Core i5 processor and 4GB 1600 MHz DDR3 memory.

4.1 3-RSMDS and fJOFC

As mentioned previously, fJOFC can be viewed as a softly constrained version of 3-RSMDS. Herein, through a simple illustrative experiment, we highlight the advantages (and disadvantages) of the fJOFC framework. Let $Y \in \mathbb{R}^{400 \times 2}$ have rows which are independent 2-dimensional Gaussian $((5, 5), I_2)$ random variables. Letting $z = \max(Y) - \min(Y)$, for $i = 1, 2, 3$, we set Y_i to be $Y + E_i$, with the entries of E_i being independent Uniform $(-z/50, z/50)$ random variables, which are also independent across i . We set Δ_i to be the interpoint distance matrix of Y_i . These $\{Y_i\}$ represent our $n = 400$ objects measured under $m = 3$ modalities. Let $Z \in \mathbb{R}^{400 \times 2}$ have rows 11, 12, \dots , 400 identical to those in Y and let the

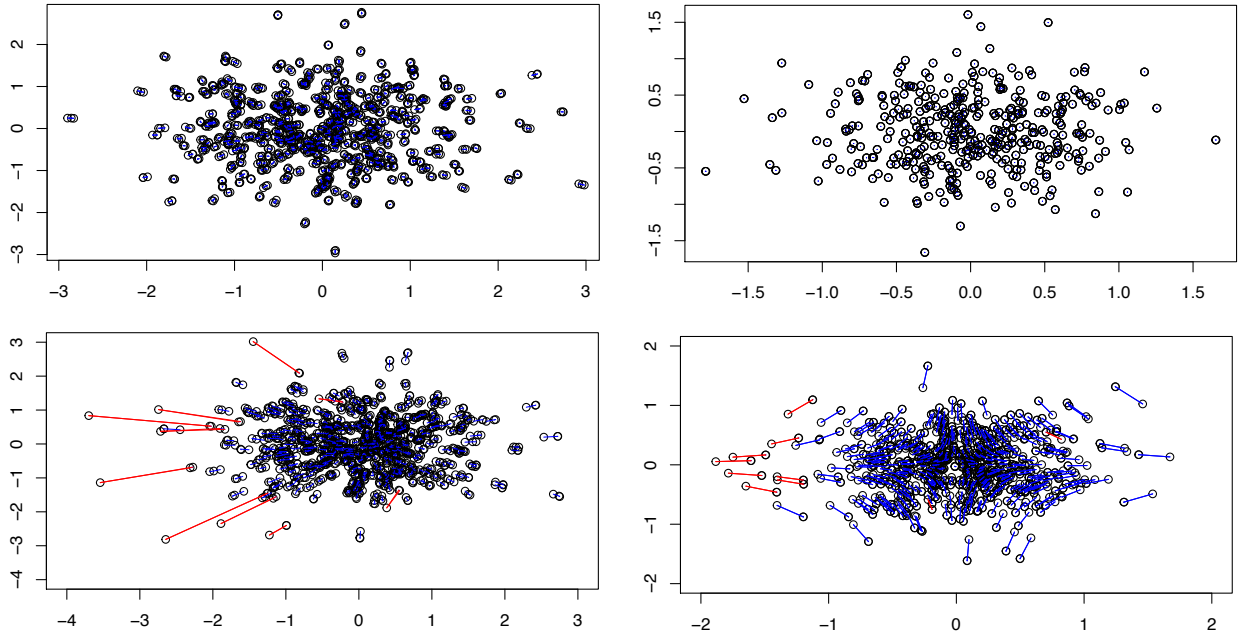


Figure 1: For a single Monte Carlo iterate, we plot the embeddings of the three dissimilarities in the matched (top row, left panel is fJOFC, right panel is 3-MDS) and the anomaly (bottom row, left panel is fJOFC, right panel is 3-MDS) settings. In the matched setting, matched triplets are connected by blue lines. In the anomaly setting, blue lines connect the matched points across the embeddings and red lines connect the ten anomaly points they are “matched” to in the data.

first ten rows of Z be independent 2-dimensional Gaussian $((8, 8), 2 \cdot I_2)$ random variables. Let $Y_4 = Z + E_4$, with E_4 defined analogously to the E_i 's above. Let Δ_4 be the interpoint distance matrix of Y_4 .

We use fJOFC and the INDSCAL algorithm (for 3-RSMDS, as implemented in the `smacof` package (Leeuw and Mair, 2008) in `R`) to embed $(\Delta_1, \Delta_2, \Delta_3)$ (the matched setting) and $(\Delta_1, \Delta_2, \Delta_4)$ (the anomaly setting). Results are summarized below in Figure 1 and Table 2. In Figure 1, for a single Monte Carlo iterate, we plot the embeddings of the three dissimilarities in the matched (top row, left panel is fJOFC, right panel is 3-MDS) and the anomaly (bottom row, left panel is fJOFC, right panel is 3-MDS) settings. In the matched setting, matched triplets are connected by blue lines. In the anomaly setting, blue lines connect the matched points across the embeddings and red lines connect the ten anomaly points they are “matched” to in the data.

Method	Runtime1	Stress1	ARI	Runtime2	Stress2	ARI2	Conf. Ratio
3-RSMDS	214.52	0.042	0.69	312.39	0.18	0.40	10.29
fJOFC	1.39	0.03	0.66	11.56	0.16	0.57	76.07

Table 2: The average running time (over 25 MC iterates) is shown as Runtime1 (in the matched setting) and Runtime2 (in the anomaly setting). The average final normalized stress is Stress1 (in the matched setting) and Stress2 (in the anomaly setting). In the matched setting, the ARI gives the a measure of the fidelity of the K -means clustering of the data into 400 clusters (each should contain the three jitters of the same point). In the anomaly setting, the ARI2 column gives a measure of the fidelity of the K -means clustering of the non-anomalous data into 390 clusters (each should contain the three jitters of the same point). Lastly, the Conf. Ratio column gives the ratio of the average distance between the triplets of points that have the anomalies (the ten outlier triplets) and the triplets that are correctly matched in the anomaly setting (the 390 non-outlier triplets).

Results over 25 MC iterates are summarized in Table 2. The average running time is shown as Runtime1 (in the matched setting) and Runtime2 (in the anomaly setting). The average final normalized stress is Stress1 (in the matched setting) and Stress2 (in the anomaly setting). In the matched setting, the ARI (adjusted Rand index; see Hubert and Arabie (1985)) a measure of the fidelity of the K -means clustering of the data into 400 clusters (each should contain the three jitters of the same point). In the anomaly setting, the column ARI2 gives the a measure of the fidelity of the K -means clustering of the non-anomalous data into 390 clusters (each should contain the three jitters of the same non-anomalous point). An ARI of 1 means that the clustering of the embedded points perfectly clusters the repeated observations of the data, while an ARI of 0 indicates that the clustering of the embedded points behaves as chance in recovering the clusters of the repeated observations. Lastly, the Conf. Ratio column gives the ratio of the average distance between the triplets of points that have the anomalies (the ten anomaly triplets) and the triplets that are correctly matched in the anomaly setting (the 390 non-anomaly triplets). From this simple experiment, we see that fJOFC is empirically i. much faster than (this off the shelf implementation of) 3-RSMDS; ii. performs comparably to 3-RSMDS

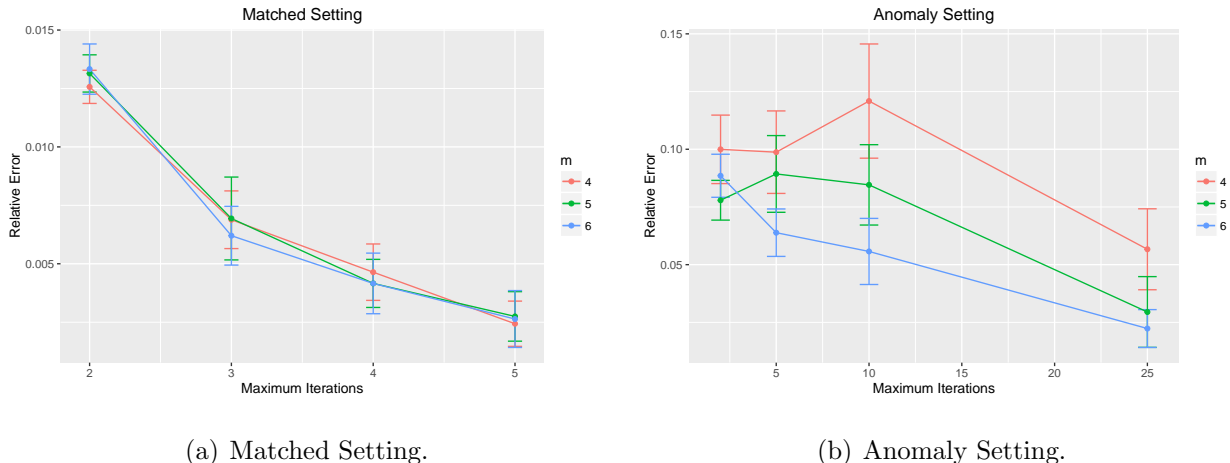


Figure 2: We plot the average (over 25 Monte Carlo iterates) relative error $\frac{\|\mathbf{X}_{(\text{final})} - \mathbf{X}_{(k)}\|_2}{\|\mathbf{X}_{(\text{final})}\|_2} \pm 2$ s.e. over a range of values of k (the x -axis in Figure 2(a)). In the left panel, we plot the ratio in the matched setting with $m = 4, 5, 6$ dissimilarities and in the right panel, we plot the ratio in the anomaly setting with $m = 4, 5, 6$ dissimilarities, one of which contains the anomaly. Note that in the anomaly setting, only the relative error amongst the $n * (m - 1) + (n - 10)$ non-anomalous points is plotted.

when the data are all matched across the modalities with no anomalous behavior—see the ARI column in Table 2; iii. is better able to preserve the correct matchedness in the presence of anomalous data—see the ARI2 and Conf. Ratio columns of Table 2; results which are echoed in Sun and Priebe (2013); Shen et al. (2016)

4.2 Error tolerance

With the same setting as in Section 4.1, we explore the effect of early stopping on the global fJOFC output. As mentioned previously, the sequential Guttman transforms often exhibit good global properties, and good solutions can often be obtained after only a few iterates. To demonstrate this, we plot the relative error (over 25 Monte Carlo iterates) $\frac{\|\mathbf{X}_{(\text{final})} - \mathbf{X}_{(k)}\|_2}{\|\mathbf{X}_{(\text{final})}\|_2} \pm 2$ s.e. over a range of values of k (the x -axis in Figure 2(a)). In the left panel, we plot the ratio in the matched setting with $m = 4, 5, 6$ dissimilarities and in the right panel, we plot the ratio in the anomaly setting with $m = 4, 5, 6$ dissimilarities, one

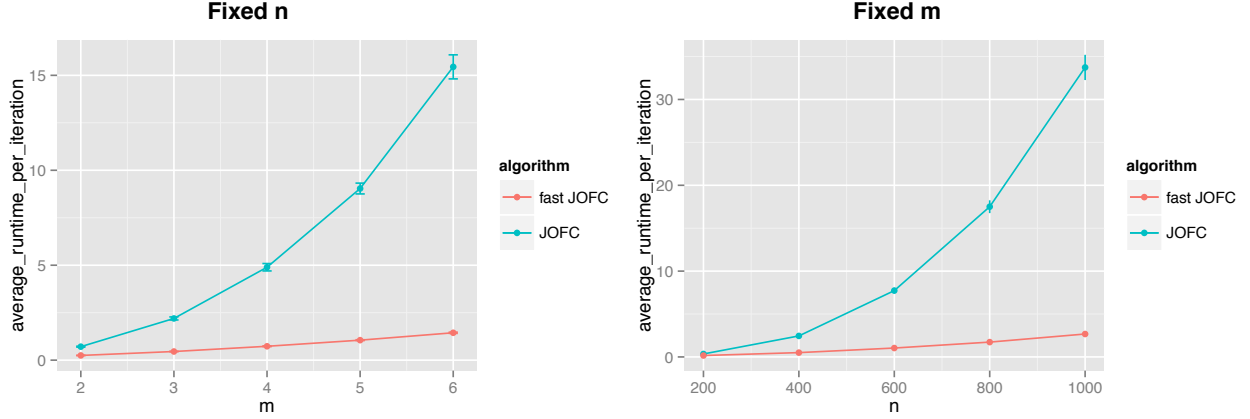


Figure 3: We embed $\Delta \in \mathbb{R}^{nm \times nm}$ via fJOFC and JOFC using identical initial configurations $\mathbf{X}_{(0)} = \text{cMDS}(\Delta)$ as in Remark 2. We then plot the average run time (in seconds) per iteration ($\pm 2s.e.$) versus m (left panel) and n (right panel) for both JOFC and fJOFC, averaged over 50 Monte Carlo replicates. In the left panel we fix $n = 400$, and vary $m = 2, 3, 4, 5, 6$. In the right panel, we fix $m = 3$ and vary $n = 200, 400, 600, 800, 1000$.

of which contains the anomaly. Note that in the anomaly setting, only the relative error amongst the $n * (m - 1) + (n - 10)$ non-anomalous points is plotted. We see that, in the matched setting, very few sequential iterates are needed before the embedding stabilizes. In the anomaly setting—when on average over 100 sequential iterates are needed for the algorithm to terminate with $\epsilon = 10^{-6}$ tolerance—we see $\approx 5\%$ relative error with only 25 iterates. Indeed, here and in the real data examples, we find that $\epsilon = 10^{-6}$ is often a conservative tolerance level and a sufficiently good embedding can be obtained with far fewer iterates; we are presently investigating methods for adaptively choosing the number of iterates, though we do not pursue this further here.

4.3 JOFC versus fJOFC

Let $Y \in \mathbb{R}^{400 \times 2}$ have rows which are independent 2-dimensional Gaussian($((5, 5), I_2)$) random variables. Letting $z = \max(Y) - \min(Y)$, for $i = 1, 2, \dots, 6$, we set Y_i to be $Y + E_i$, with the entries of E_i being independent Uniform($-z/50, z/50$) random variables, which are also independent across i . We set Δ_i to be the interpoint distance matrix of Y_i . These $\{Y_i\}$ represent our $n = 400$ objects measured under $m = 6$ modalities. For $m = 2, 3, \dots, 6$, we

embed the omnibus matrix Δ (defined as in Section 1.2.1) into \mathbb{R}^2 with both fJOFC (in serial) and JOFC using an identical initial configurations $\mathbf{X}_{(0)} = \text{cMDS}(\Delta)$, as outlined in Remark 2. We plot the average run time per iteration versus m for both fJOFC and JOFC in Figure 3 (left panel), averaged over 50 Monte Carlo replicates. Even in this relatively small simulation, the decreased runtime speed is dramatically illustrated, even with fJOFC run in serial. The ratio of the average run times (JOFC versus fJOFC) is (2.86, 4.82, 6.70, 8.59, 10.71) for $m = (2, 3, 4, 5, 6)$, which suggests that fJOFC is a factor of m ($\approx 1.6m$) faster than JOFC here. This corroborates the runtime results in Section 2; indeed, as here n is constant, JOFC has complexity $O(m^3)$ while fJOFC has complexity $O(m^2)$.

We next consider the case of fixed $m = 3$ and varying $n = (200, 400, 600, 800, 1000)$. With Y and Δ defined as above, we again embed $\Delta \in \mathbb{R}^{nm \times nm}$ into \mathbb{R}^2 via fJOFC (in serial) and JOFC using identical initial configurations $\mathbf{X}_{(0)} = \text{cMDS}(\Delta)$. In Figure 3 (right panel), we plot the average run time per iteration versus n for both JOFC and fJOFC, averaged over 50 Monte Carlo replicates. Again, note the dramatic speedup achieved by fJOFC, with the ratio of the average run times (JOFC versus fJOFC) being (2.10, 4.86, 7.45, 10.13, 12.63) for $n = (200, 400, 600, 800, 1000)$. This suggests that fJOFC is a factor of n ($\approx 0.12n$) faster than JOFC here, which corroborates the runtime results in Section 2; indeed, as here m is constant, JOFC has complexity $O(n^3)$ while fJOFC has complexity $O(n^2)$.

4.4 Out-of-sample efficiency

We next demonstrate the efficiency of the out-of-sample fJOFC procedure. With the same data set-up as above (with 3-dimensional Gaussian random variables here, but otherwise identical to the data setup used above), we embed all but one object of $\Delta \in \mathbb{R}^{nm \times nm}$ via fJOFC, and use the out-of-sample procedure to embed the final object (m views of the n -th object). Running time results (in seconds) are plotted in Figure 4, where we plot the average running time (in seconds) $\pm 2s.e.$ of the in-sample and the out-of-sample procedure versus m (left panel) and versus n (right panel), averaged over 25 Monte Carlo replicates. In the left panel we fix $n = 200$, and vary $m = 10, 15, 20, 25, 30$. In the right panel, we fix $m = 10$ and vary $n = 200, 300, 400, 500, 600$. As seen previously, the runtime of fJOFC

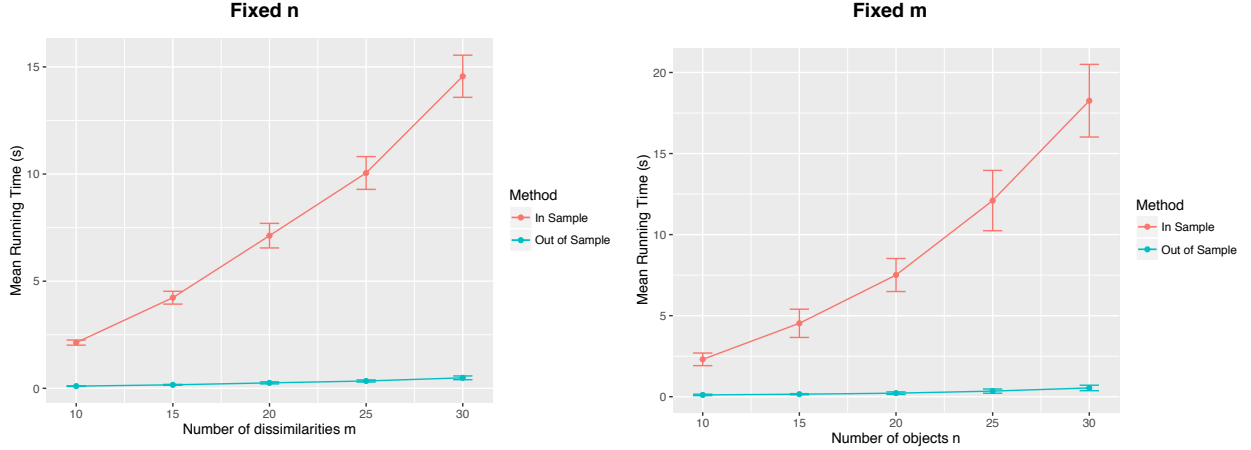


Figure 4: We embed all but one object of $\Delta \in \mathbb{R}^{nm \times nm}$ via fJOFC, and use the out-of-sample procedure to embed the final object (m views of the n -th object). We then plot the average running time (in seconds) $\pm 2s.e.$ of the in-sample and the out-of-sample procedure versus m (left panel) and versus n (right panel), averaged over 25 Monte Carlo replicates. In the left panel we fix $n = 200$, and vary $m = 10, 15, 20, 25, 30$. In the right panel, we fix $m = 10$ and vary $n = 200, 300, 400, 500, 600$.

empirically varies quadratically (in n for fixed m and in m for fixed n). However, we observe that the runtime of the out-of-sample procedure empirically varies linearly (in n for fixed m and in m for fixed n), which agrees with the computational complexity results of Section 3.

In Table 3 we show the sum of the residual errors of the out-of-sample embedding versus the in-sample embedding— $\sum_{i=1}^m \|\mathbf{X}_{(\text{final})}^{(i)}[n, :] - \mathbf{y}_i\|_2$ —for fixed n and varying m (top row) and for fixed m and varying n (bottom row) averaged over 25 Monte Carlo iterates. For each combination of m and n , we first embed the full $mn \times mn$ dissimilarity Δ using fJOFC. We next embed all but one of the objects ($n - 1$ objects over m modalities) using fJOFC and the n -th object via the out-of-sample procedure of Section 3, and compute the sum of the residual errors between the out-of-sample and the in-sample embeddings of the n -th object. We see that, for fixed n and varying m , the total error is increasing in m but negligible on average per modality. As m is fixed and n varies, the total error is relatively constant, which is unsurprising as, in each case, exactly m additional data points are being out-of-sample embedded into a fixed dimensional space.

Sum of Residual Errors of Out-of-Sample Versus In-Sample

	$m = 10$	$m = 15$	$m = 20$	$m = 25$	$m = 30$
$n = 200$	0.067	0.121	0.184	0.366	0.364
	$n = 200$	$n = 300$	$n = 400$	$n = 500$	$n = 600$
$m = 10$	0.057	0.059	0.101	0.078	0.091

Table 3: The sum of the residual errors of the out-of-sample embedding versus the in-sample embedding— $\sum_{i=1}^m \|\mathbf{X}_{(\text{final})}^{(i)}[n, :] - \mathbf{y}_i\|_2$ —for fixed n and varying m (top row) and for fixed m and varying n (bottom row) averaged over 25 Monte Carlo iterates.

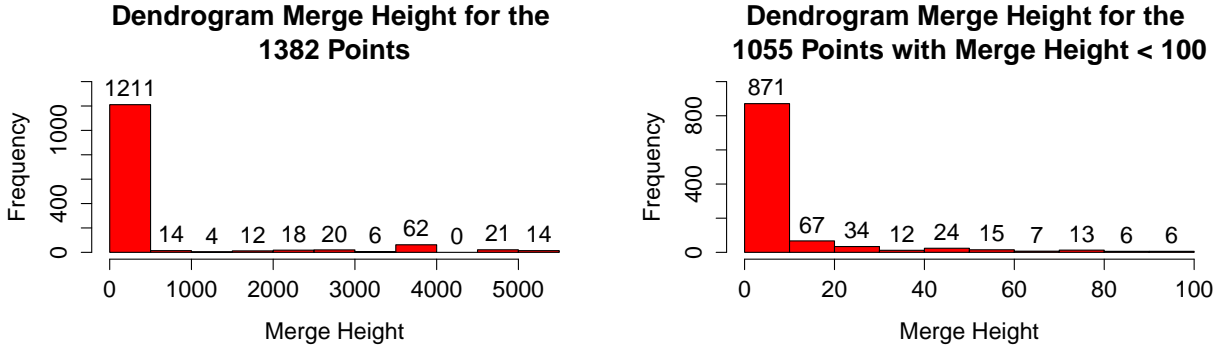
4.5 Real Data Examples

We next demonstrate the key feature of the JOFC procedure in a pair of real data sets; namely, the ability of the algorithm to preserve cross-modality matchedness while not forcing incommensurate versions of the data points to be artificially embedded close to one another. Indeed, in the JOFC procedure,

1. if an object’s properties are well-preserved across the m modalities, then the object’s associated m points in the configuration will be embedded close to each other;
2. if an object’s properties are not well-preserved across the m modalities, then JOFC (with well-chosen w) will not artificially force the object’s m incommensurate configuration points to be close to each other in the embedding.

Incommensurate embeddings can inform both how and why the data modalities differ. By studying these pathologies further, we aim to better understand the data features that are emphasized in one modality versus another, which is crucial for understanding potential benefits from pursuing further inference in the joint (versus single) embedding space.

We explore this further below in a data set derived from the French and English Wikipedia graphs and in a time series of zebrafish calcium ion brain images from Prevedel et al. (2014).



(a) Dendrogram merge heights, all $n = 1382$ points. (b) Dendrogram merge heights for the $n = 1055$ points with merge height < 100 .

Figure 5: Histograms showing, for each of the $n = 1382$ points in (a) and for each of the 1055 points with merge height < 100 in (b), the height in the hierarchical clustering dendrogram when each of the four modalities was first merged into a single cluster for that point.

4.5.1 Wikipedia

We collect the $n = 1382$ articles $\{y_{1i}\}_{i=1}^{1382}$ from English Wikipedia which compose the 2-hop neighborhood of the article entitled “Algebraic Geometry” (where articles are linked if there exists a hyperlink in one article to the other, and these links are considered undirected). There is a natural 1-1 correspondence between these articles and their versions in French Wikipedia, and we will denote the associated French articles by $\{y_{2i}\}_{i=1}^{1382}$.

As in Shen et al. (2016), each $\{y_{ji}\}_{i=1}^{1382}$ for $j = 1, 2$, further gives rise to two measures of inter-article dissimilarity: Δ_{j1} , the shortest path distance in the undirected hyperlink graph; and Δ_{j2} , the cosine dissimilarities between text feature vectors (provided by latent semantic indexing, see Deerwester et al. (1990) for detail) associated with each article. We use fJOFC—with $w = 10$ as suggested by Adali and Priebe (2015)—to embed these $n = 1382$ points across $m = 4$ modalities into \mathbb{R}^{10} . Note that implementing our fJOFC algorithm in serial ran in ≈ 42.2 minutes while the JOFC algorithm with the same settings ran in ≈ 10.37 hours (a factor of ≈ 14.7 speedup).

In this omnibus embedding, if all 4 embedded versions of a single Wikipedia article lie

close together, then this article’s relationship to all of the other articles is preserved across modality. If any of the 4 embedded versions is incommensurate with the others then this would indicate either:

- i. The text features of the article differ significantly across language; i.e. the associated row of $\mathbf{X}_i^{(2)}$, the embedding associated with Δ_{12} , is far from $\mathbf{X}_i^{(4)}$, the embedding associated with Δ_{22} . While the French articles are not translations of their English counterparts (or vice versa), further understanding the textual feature highlighted by these incommensurabilities would be useful before pursuing further inference (e.g. topic modeling) in the joint embedding.
- ii. The hyperlink graph structure is not preserved across modality; i.e. the associated row of $\mathbf{X}_i^{(1)}$, the embedding associated with Δ_{11} , is far from $\mathbf{X}_i^{(3)}$, the embedding associated with Δ_{21} .
- iii. The hyperlink structure and the textual similarities are incommensurate; i.e. the associated row of $\mathbf{X}_i^{(1)}$, the embedding associated with Δ_{11} , is far from $\mathbf{X}_i^{(2)}$, the embedding associated with Δ_{12} , or the associated row of $\mathbf{X}_i^{(3)}$, the embedding associated with Δ_{21} , is far from $\mathbf{X}_i^{(4)}$, the embedding associated with Δ_{22} . By studying these incommensurabilities further, we hope to better understand the data features that are emphasized by graph-based versus text-feature-based methodologies.

To investigate further, we proceed by hierarchically clustering (using Ward’s method, see Johnson (1967) for detail) the 4×1382 points of the omnibus embedding and then compute the pairwise cophenetic distance (the height in the resulting dendrogram at which the two points are first clustered together) between each of the points. If the dissimilarities are well preserved across modality, then the maximum cophenetic distance between two embedded versions of the same article (we call this the *Dendrogram Merge Height* or DMH) should be small.

In Figure 5(a), we plot a histogram of the DMH’s for the 1382 articles, and note that over 76% of the articles have DMH less than 100. In Figure 5(b) we see that over 63% of the articles have DMH less than 10. To further confirm that the dissimilarities are well preserved across modality, we calculated cluster labels given by the hierarchical clustering

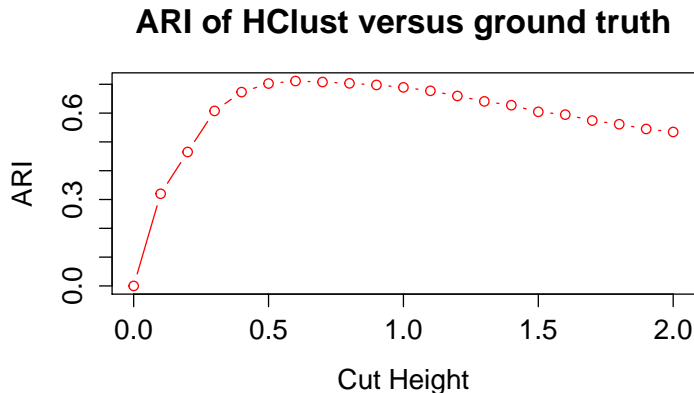


Figure 6: The adjusted Rand index between the clusters given by the hierarchical clustering dendrogram at height $h \in [0, 2]$ and the ground truth clustering (given by the 1382 size 4 clusters each composed of a single article across modalities).

dendrogram at height $h \in [0, 2]$. We then compute the adjusted Rand index, ARI (see Hubert and Arabie, 1985), between these clusterings and the ground truth clustering (given by the 1382 size 4 clusters each composed of a single article across modalities), and plot this in Figure 6. From the figure, we see that the clustering is not only grossly clustering the article 4-tuples together, but is also capturing the fine-grain differences between the different articles as well.

If the ARI between the hierarchical clustering and the ground truth clustering was equal to 1, then the structure of the four dissimilarities would be nearly identical, and joint inference across modality would yield minimal gain over separately embedding the Δ_i 's and then applying subsequent inference methodologies. From Figures 5(a)-5(b) and 6, we see this is not the case. Indeed, we see that the text-feature-based methods and graph-based methods are emphasizing some different data features both within and across language, and therefore for some articles the relative geometry in the four modality-specific embeddings is not commensurate. We illustrate this in Figure 7, where we plot a branch of the hierarchical clustering dendrogram when the tree is cut at height 20. Note that although the four modality-specific embeddings of many articles (article 454 is highlighted here in blue as an example) are very similar, some of the articles' embeddings are not preserved well across modality (article 366 is highlighted here in red as an example; note

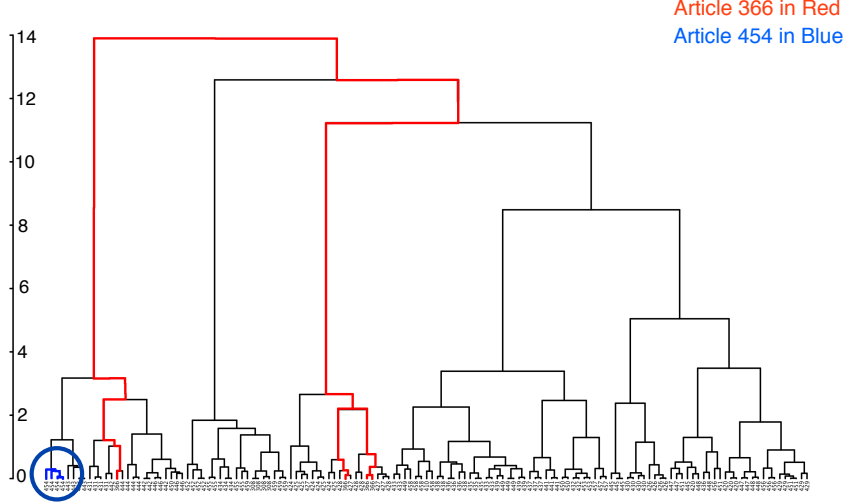


Figure 7: A branch of the hierarchical clustering dendrogram when the tree is cut at height 20. Note that the four modality-specific embeddings of article 454 (highlighted in blue in the dendrogram) are very similar, while those of article 366 are not (the English graph with shortest path distance differs significantly from the other three modalities for this point).

that the English graph with shortest path distance differs significantly from the other three modalities for this article).

4.5.2 Zebrafish brains

In Prevedel et al. (2014), the authors combined Light-Field Deconvolution Microscopy and pan-neuronal expression of GCaMP, a fluorescent calcium indicator that serves as a proxy for neuronal activity, to produce a time series of whole-brain zebrafish neuronal activity at near single neuron resolution. The data consists of 5000 realizations of a multivariate time series $\{Z^{(t)}\}_{t=1}^{5000}$ with $Z^{(t)} \in \mathbb{R}^{5379}$ for all t , where for each $i \in [5379]$, $Z^{(t)}(i) \in \mathbb{R}$ represents the activity of neuron i at time t . Each time frame $[t, t + 1)$ is 1/20 of a second; i.e. the data was collected at 20 Hz. After preprocessing the data and removing some artificial edge neurons, we are left with $Z^{(t)} \in \mathbb{R}^{5105}$ for each of $t = 1, 2, \dots, 5000$.

Binning the time stamps into 100 overlapping periods of 5 seconds (so that for each $\tau \in [100]$, bin τ consists of the matrix of observations

$$\mathbf{Z}^{(\tau)} = [Z^{(50(\tau-1)+1)} | \dots | Z^{(50(\tau+1))}] = \left[(\mathbf{Z}_1^{(\tau)})^\top | (\mathbf{Z}_2^{(\tau)})^\top | \dots | (\mathbf{Z}_{5105}^{(\tau)})^\top \right]^\top \in \mathbb{R}^{5105 \times 100},$$

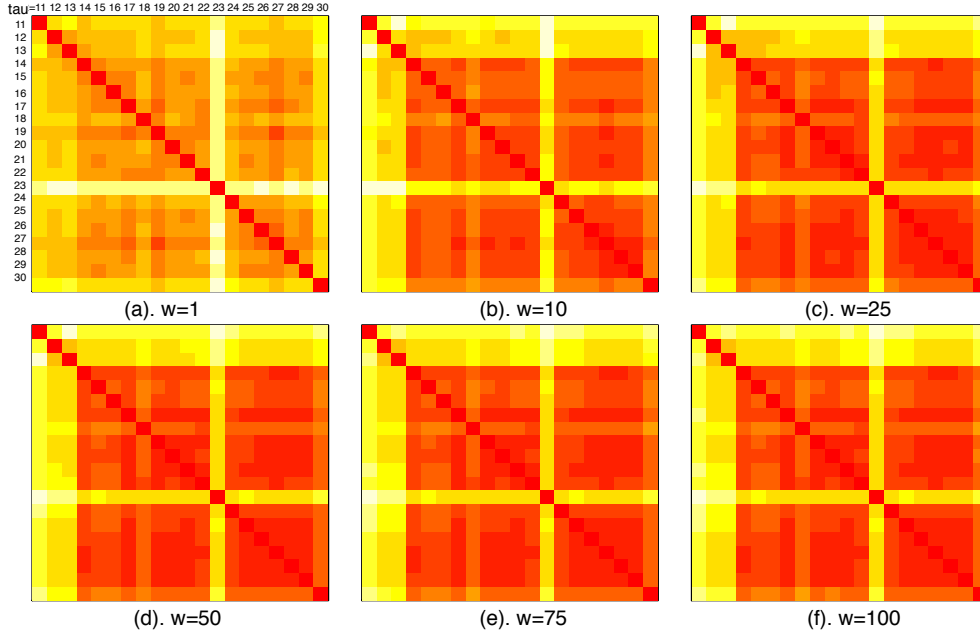


Figure 8: Heatmaps of the Frobenius norm differences between the 20 zebrafish neuron embeddings $\{\mathbf{X}^{(\tau)}\}_{\tau=11}^{30}$ obtained by fJOFC over a range of w 's. Each heatmap is a 20×20 grid, where the intensity of the i, j -th entry indicates the difference between the embeddings of the n^* fish neurons at times $\tau = i$ and $\tau = j$; more red indicates less difference in the embedded space and white indicating very different embeddings. Note the anomalous point at $\tau = 23$.

we compute a time series of 100 dissimilarity matrices $\{\Delta^{(\tau)}\}_{\tau=1}^{100}$ as follows. For each τ , we compute the thresholded correlation matrix $D^{(\tau)} \in \mathbb{R}^{5105 \times 5105}$ with

$$D_{i,j}^{(\tau)} = \mathbb{1}\{|\text{corr}(\mathbf{Z}_i^{(\tau)}, \mathbf{Z}_j^{(\tau)})| > 0.7\}$$

(where the threshold 0.7 was chosen to ensure sufficient sparsity in the resulting $D^{(\tau)}$'s). These correlation matrices are then transformed to dissimilarity matrices $\{\Delta^{(\tau)}\}_{\tau=1}^{100}$ by defining

$$\Delta_{i,j}^{(\tau)} = 1 - \frac{|N_{\tau}(i) \cap N_{\tau}(j)|}{|N_{\tau}(i) \cup N_{\tau}(j)|},$$

where $N_{\tau}(i)$ is the neighborhood of neuron i in $D^{(\tau)}$ viewed as a graph.

Initial change point detection analysis, analogous to that in Park et al. (2015), indicated that there was an anomaly in the neural correlations at time $\tau^* = 23$ and identified $n^* = 469$ neurons responsible for this anomaly. To explore this further, we use fJOFC to embed a

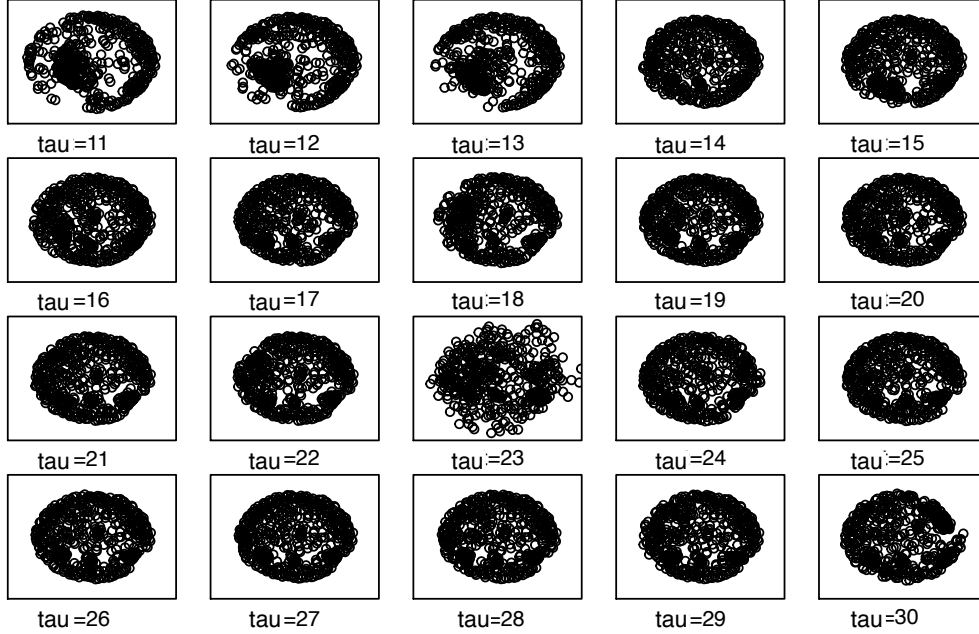


Figure 9: Embeddings of the $m = 20$ elements of the time-series $\{\tilde{\Delta}^{(\tau)}\}_{\tau=11}^{30}$ into \mathbb{R}^2 obtained via fJOFC with $w = 10$. Each of the 20 plots is on the same set of axes. Note the anomaly at $\tau = 23$.

portion of the time series (from times $\tau = 11$ to $\tau = 30$) obtaining the configuration

$$\mathbf{X}^\top = [(\mathbf{X}^{(11)})^\top | (\mathbf{X}^{(12)})^\top | \dots | (\mathbf{X}^{(30)})^\top]^\top.$$

If there is an anomaly in the activity of the n^* neurons at $\tau^* = 23$, this should be evinced by $\mathbf{X}^{(23)}$ significantly differing from $\mathbf{X}^{(\tau)}$ for $\tau \neq 23$, as seen in Figures 8 and 9. Moreover, the embedding can also inform the *structure* of the anomaly, as we can identify the change in structure within the $n^* = 469$ neurons which is responsible for the anomaly in the embedded space; see Figure 10. Below, we expound on the details of our embedding procedure and findings.

Restricting the full dissimilarities to the n^* identified anomalous neurons—yielding a times series $\{\tilde{\Delta}^{(\tau)}\}_{\tau=1}^{100}$ of 100 dissimilarities in $\mathbb{R}^{469 \times 469}$ —we first embed the $m = 20$ elements of $\{\tilde{\Delta}^{(\tau)}\}_{\tau=11}^{30}$ into \mathbb{R}^2 . To test if there is an anomaly at $\tau = 23$, we next compute the Frobenius norm differences between the 20 embeddings $\{\mathbf{X}^{(\tau)}\}_{\tau=11}^{30}$ in the configuration. Results are summarized in Figure 8, where we plot a heatmap of the Frobenius norm differences between the $\{\mathbf{X}^{(\tau)}\}_{\tau=11}^{30}$ over a range of w 's (plots of the 2-dimensional fJOFC

embeddings with $w = 10$ across $\tau = 11, 12, \dots, 30$ are displayed in Figure 9). Each heatmap is a 20×20 grid, where the intensity of the i, j -th entry indicates the difference between the embeddings of the n^* fish neurons in $\mathbf{X}^{(i)}$ and $\mathbf{X}^{(j)}$; more red indicates less difference in the embedded space and white indicating very different embeddings. We see that, across the range of w 's, there is a significant anomaly in the embedding at $\tau = 23$. This both confirms the initial findings of an anomaly at $\tau = 23$ and demonstrates the potential robustness of this anomaly-detection procedure to misspecified w . We also note that the embeddings at times $\tau = 11, 12, 13$ are significantly different from the embeddings at all other times. Further analysis is needed to determine if this is neuroscientifically significant or a data collect/algorithmic artifact. We lastly note that this embedding ran in ≈ 1.5 hours using fJOFC run in serial and over 20 hours using JOFC, again showing the dramatic speedup of our fJOFC procedure.

To further understand the structure of this anomaly, we plot the change in the embeddings from times 21–22, times 22–23, times 23–24, and times 24–25 in Figure 10 (so that there are $2n^*$ points in each panel). In the figure, the neurons in the configuration at time 23 are displayed as red points, with neurons in the configuration at other times displayed as black points. For each individual neuron, the movement in the configuration from times τ to $\tau + 1$ are highlighted with blue lines; i.e., there is a line connecting the position of the neuron at time τ to its position at time $\tau + 1$. From this figure, we can identify the groups of neurons whose change in activity is responsible for the anomaly. Again, further analysis is necessary to determine the potential neuroscientific significance of these neurons' activity.

5 Conclusion

The JOFC algorithm has proven to be a valuable and adaptable tool for a variety of inference tasks (e.g., graph matching (Lyzinski et al., 2013); hypothesis testing (Priebe et al., 2013); joint classification (Sun and Priebe, 2013); among others). The key capability enabled by our fJOFC algorithm (both in-sample and out-of-sample) versus the JOFC algorithm is enhanced scalability in m and n ; indeed, for a fixed n , we see a factor of m speedup over the JOFC algorithm, and for a fixed m we see a factor of n speed up achieved by fJOFC. Additionally, the out-of-sample fJOFC procedure is shown to have

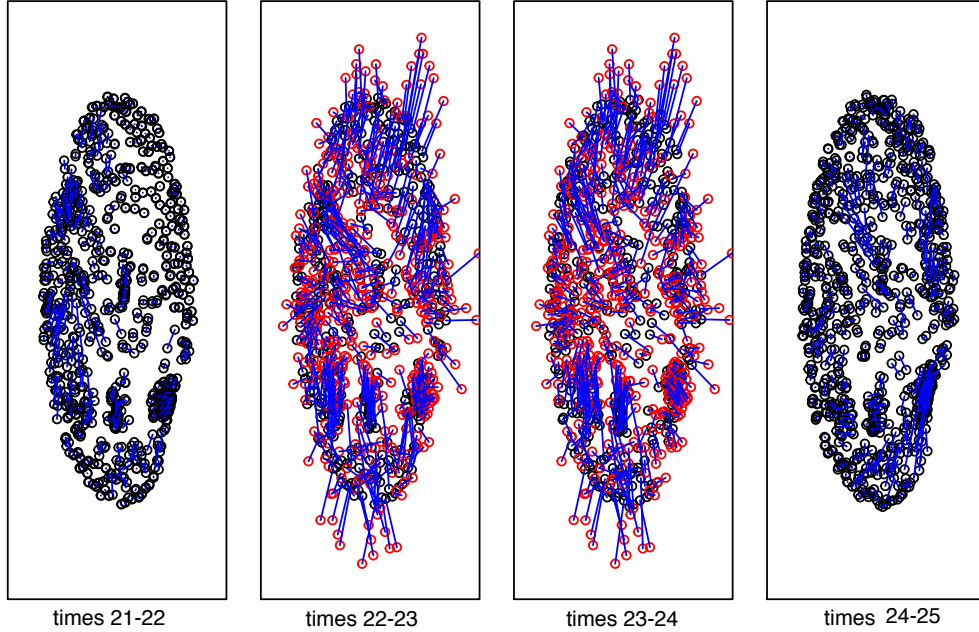


Figure 10: Plot of the change in the embeddings from times 21–22, times 22–23, times 23–24, and times 24–25 (so that there are $2n^*$ points in each panel). In the figure, the neurons in the configuration at time 23 are displayed as red points, with neurons in the configuration at other times displayed as black points. For each individual neuron, the movement in the configuration from times τ to $\tau + 1$ are highlighted with blue lines; i.e., there is a line connecting the position of the neuron at time τ to its position at time $\tau + 1$.

linear runtime in n . Combined with sparse dissimilarity representations of very large data sets, this capability to simultaneously embed many different large dissimilarities, both in and out-of-sample, enables the complex structure of the data to more easily be interrogated, leading to potentially significant discoveries heretofore beyond our grasp.

While the sequential Guttman transforms computed in Algorithm 1 are only guaranteed to converge to a stationary configuration, because the sequence of raw stress values is decreasing, in practice they will typically converge to a local minimizer of $\sigma(\mathbf{X})$. Note that, in most cases, the local convergence rate of the iterative Guttman transforms is linear, see de Leeuw (1988). In practice, the sequential Guttman transforms often exhibit good global properties, and only a few iterations are required to obtain a sufficiently good suboptimal embedding, see Kearsley et al. (1995). Analyzing these global properties and/or modifying fJOFC to accelerate the linear convergence—for example, by incorporating relaxed updates

in the iterative majorization as in De Leeuw and Heiser (1980)—are essential next steps for further scaling fJOFC to very big data.

A Derivation of \mathbf{L}^\dagger

In this section, we collect supporting results to derive the desired form of \mathbf{L}^\dagger . We first prove that \mathbf{L}^\dagger can be realized via $\mathbf{L}^\dagger = \left(\mathbf{L} + \frac{1}{mn}J_{mn}\right)^{-1} - \frac{1}{mn}J_{mn}$,

Proposition 9. *Let \mathbf{W} be any symmetric weight matrix in $\mathbb{R}^{mn \times mn}$. If \mathbf{L} is the combinatorial Laplacian of \mathbf{W} , then \mathbf{L} can be equivalently realized via*

$$\mathbf{L}^\dagger = \left(\mathbf{L} + \frac{1}{mn}J_{mn}\right)^{-1} - \frac{1}{mn}J_{mn}. \quad (17)$$

Proof. The proof is straightforward linear algebra, but we include it here for completeness.

We first note that $J_{mn}\mathbf{L} = \mathbf{L}J_{mn} = 0$, so that

$$\left(\mathbf{L} + \frac{1}{mn}J_{mn}\right)J_{mn} = J_{mn} = J_{mn}\left(\mathbf{L} + \frac{1}{mn}J_{mn}\right).$$

We then calculate

$$\begin{aligned} \mathbf{L} \left[\left(\mathbf{L} + \frac{1}{mn}J_{mn}\right)^{-1} - \frac{1}{mn}J_{mn} \right] \mathbf{L} &= \mathbf{L} \left(\mathbf{L} + \frac{1}{mn}J_{mn}\right)^{-1} \mathbf{L} \\ &= \mathbf{L} \left(\mathbf{L} + \frac{1}{mn}J_{mn}\right)^{-1} \left(\mathbf{L} + \frac{1}{mn}J_{mn} - \frac{1}{mn}J_{mn}\right) \\ &= \mathbf{L} \left(I_{mn} - \frac{1}{mn}J_{mn}\right) = \mathbf{L}; \end{aligned}$$

and

$$\begin{aligned} &\left[\left(\mathbf{L} + \frac{1}{mn}J_{mn}\right)^{-1} - \frac{1}{mn}J_{mn} \right] \mathbf{L} \left[\left(\mathbf{L} + \frac{1}{mn}J_{mn}\right)^{-1} - \frac{1}{mn}J_{mn} \right] \\ &= \left[\left(\mathbf{L} + \frac{1}{mn}J_{mn}\right)^{-1} - \frac{1}{mn}J_{mn} \right] \left(\mathbf{L} + \frac{1}{mn}J_{mn} - \frac{1}{mn}J_{mn}\right) \left[\left(\mathbf{L} + \frac{1}{mn}J_{mn}\right)^{-1} - \frac{1}{mn}J_{mn} \right] \\ &= \left[I_{mn} - 2\frac{1}{mn}J_{mn} + \frac{1}{mn}J_{mn} \right] \left[\left(\mathbf{L} + \frac{1}{mn}J_{mn}\right)^{-1} - \frac{1}{mn}J_{mn} \right] = \left(\mathbf{L} + \frac{1}{mn}J_{mn}\right)^{-1} - \frac{1}{mn}J_{mn}; \end{aligned}$$

and $\left[\left(\mathbf{L} + \frac{1}{mn}J_{mn}\right)^{-1} - \frac{1}{mn}J_{mn} \right] \mathbf{L} = I_{mn} - \frac{1}{mn}J_{mn} = \mathbf{L} \left[\left(\mathbf{L} + \frac{1}{mn}J_{mn}\right)^{-1} - \frac{1}{mn}J_{mn} \right]$ is Hermitian. It follows that $\mathbf{L}^\dagger = \left(\mathbf{L} + \frac{1}{mn}J_{mn}\right)^{-1} - \frac{1}{mn}J_{mn}$ as desired. \square

We have that the combinatorial Laplacian of \mathbf{W} is given by $\mathbf{L} = \mathcal{W} \otimes I_n - \text{diag}(w_{i,i}) \otimes J_n$.

It follows that

$$\mathbf{L} + \frac{1}{mn} J_{mn} = \mathcal{W} \otimes I_n + \left(\frac{1}{mn} J_m - \text{diag}(w_{i,i}) \right) \otimes J_n.$$

Proposing that $(\mathbf{L} + \frac{1}{mn} J_{mn})^{-1}$ is of the form $\mathcal{V} \otimes I_n + \mathcal{Z} \otimes J_n$, we arrive at the following.

Theorem 10. *With notation as above, let \mathbf{W} be a weight matrix of the form of Eq. (9), and assume that $w_{i,i} > 0$ for all $i \in \{1, 2, \dots, m\}$. Let \mathbf{L} be the combinatorial Laplacian of \mathbf{W} , then*

$$\left(\mathbf{L} + \frac{1}{mn} J_{mn} \right)^{-1} = \left(\mathcal{W} \otimes I_n + \left(\frac{1}{mn} J_m - \text{diag}(w_{i,i}) \right) \otimes J_n \right)^{-1} = \mathcal{V} \otimes I_n + \mathcal{Z} \otimes J_n,$$

where $\mathcal{V} = \mathcal{W}^{-1}$ and $\mathcal{Z} = - \left(\mathcal{W} + n \left(\frac{1}{mn} J_m - \text{diag}(w_{i,i}) \right) \right)^{-1} \left(\frac{1}{mn} J_m - \text{diag}(w_{i,i}) \right) \mathcal{W}^{-1}$.

Proof. First note that the assumption on $\{w_{i,i}\}_{i=1}^m$ assures that \mathcal{W} is strictly diagonally dominant and is therefore invertible. If the proposed form, $(\mathbf{L} + \frac{1}{mn} J_{mn})^{-1} = \mathcal{V} \otimes I_n + \mathcal{Z} \otimes J_n$, is correct then

$$\begin{aligned} I_{mn} &= \left(\mathbf{L} + \frac{1}{mn} J_{mn} \right) \left(\mathbf{L} + \frac{1}{mn} J_{mn} \right)^{-1} \\ &= \left(\mathcal{W} \otimes I_n + \left(\frac{1}{mn} J_m - \text{diag}(w_{i,i}) \right) \otimes J_n \right) (\mathcal{V} \otimes I_n + \mathcal{Z} \otimes J_n) \\ &= (\mathcal{W}\mathcal{V}) \otimes I_n + \left(\left(\mathcal{W} + n \left(\frac{1}{mn} J_m - \text{diag}(w_{i,i}) \right) \right) \mathcal{Z} + \left(\frac{1}{mn} J_m - \text{diag}(w_{i,i}) \right) \mathcal{V} \right) \otimes J_n \end{aligned}$$

From this, the desired forms of \mathcal{V} and \mathcal{Z} follow immediately. \square

From Theorem 10, the following Corollary is immediate:

Corollary 11. *With notation as above, let \mathbf{W} be a weight matrix of the form of Eq. (9), and assume that $w_{i,i} > 0$ for all $i \in \{1, 2, \dots, m\}$. Let \mathbf{L} be the combinatorial Laplacian of \mathbf{W} , then*

$$\mathbf{L}^\dagger = \mathcal{W}^{-1} \otimes I_n + \left[- \left(\mathcal{W} + n \left(\frac{J_m}{mn} - \text{diag}(w_{i,i}) \right) \right)^{-1} \left(\frac{J_m}{mn} - \text{diag}(w_{i,i}) \right) \mathcal{W}^{-1} - \frac{J_m}{mn} \right] \otimes J_n.$$

References

- Adali, S. and Priebe, C. E. (2015), “Fidelity-Commensurability Tradeoff in Joint Embedding of Disparate Dissimilarities,” *Journal of Classification*, To appear.
- Borg, I. and Groenen, P. J. F. (2005), *Modern Multidimensional Scaling: Theory and Applications*, Springer.
- Carroll, J. D. and Chang, J.-J. (1970), “Analysis of individual differences in multidimensional scaling via an N-way generalization of Eckart-Young decomposition,” *Psychometrika*, 35, 283–319.
- Carroll, J. D. and Wish, M. (1974), “Models and methods for three-way multidimensional scaling,” *Contemporary developments in mathematical psychology*, 2, 57–105.
- Castle, B. (2012), “Quasi-newton methods for stochastic optimization and proximity-based methods for disparate information fusion,” Ph.D. thesis, Indiana University, Department of Computer Science.
- de Leeuw, J. (1988), “Convergence of the majorization method for multidimensional scaling,” *Journal of Classification*, 5, 163–180.
- De Leeuw, J. and Heiser, W. J. (1980), “Multidimensional scaling with restrictions on the configuration,” *Multivariate analysis*, 5, 501–522.
- Deerwester, S. C., Dumais, S. T., Landauer, T. K., Furnas, G. W., and Harshman, R. A. (1990), “Indexing by latent semantic analysis,” *JASIS*, 41, 391–407.
- Elgammal, A. and Lee, C.-S. (2004), “Inferring 3D body pose from silhouettes using activity manifold learning,” in *Proceedings of the 2004 IEEE Computer Society Conference on Computer Vision and Pattern Recognition, 2004*, IEEE, vol. 2, pp. II–681.
- Gower, J. C. (2006), “An application of the modified Leverrier–Faddeev algorithm to the spectral decomposition of symmetric block-circulant matrices,” *Computational Statistics and Data Analysis*, 50, 89–106.

- Gower, J. C. and Groenen, P. J. F. (1990), “Applications of the Modified Leverrier-Faddeev Algorithm for the Construction of Explicit Matrix Spectral Decompositions and Inverses,” Tech. rep., University of Leiden.
- Ham, J., Lee, D. D., and Saul, L. K. (2005), “Semisupervised alignment of manifolds.” in *AISTATS*, pp. 120–127.
- Ham, J. H., Lee, D. D., and Saul, L. K. (2003), “Learning high dimensional correspondences from low dimensional manifolds,” in *ICML*.
- Hardoon, D., Szedmak, S., and Shawe-Taylor, J. S. (2004), “Canonical correlation analysis: An overview with application to learning methods,” *Neural Computation*, 16, 2639–2664.
- Harshman, R. A. and Lundy, M. E. (1984), “The PARAFAC model for three-way factor analysis and multidimensional scaling,” *Research methods for multimode data analysis*, 122–215.
- Heiser, W. (1988), “PROXSCAL, multidimensional scaling of proximities,” in *International meeting on the analysis of multiway data matrices, software guide*, pp. 77–81.
- Hubert, L. and Arabie, P. (1985), “Comparing partitions,” *Journal of Classification*, 2, 193–218.
- Johnson, S. C. (1967), “Hierarchical clustering schemes,” *Psychometrika*, 32, 241–254.
- Karakos, D., Eisner, J., Khudanpur, S., and Priebe, C. E. (2007), “Cross-Instance Tuning of Unsupervised Document Clustering Algorithms.” in *HLT-NAACL*, Citeseer, pp. 252–259.
- Kearsley, A. J., Tapia, R. A., and Trosset, M. W. (1995), “The solution of the metric STRESS and SSTRESS problems in multidimensional scaling using Newton’s method,” Tech. rep., DTIC Document.
- Lafon, S., Keller, Y., and Coifman, R. R. (2006), “Data fusion and multicue data matching by diffusion maps,” *Pattern Analysis and Machine Intelligence, IEEE Transactions on*, 28, 1784–1797.

- Leeuw, J. d. and Mair, P. (2008), “Multidimensional scaling using majorization: SMACOF in R,” .
- Lyzinski, V., Adali, S., Vogelstein, J. T., and Priebe, C. (2013), “Seeded Graph Matching via Joint Optimization of Fidelity and Commensurability,” *arXiv preprint, arXiv:1401.3813*.
- Ma, Z. (2010), “Disparate information fusion in the dissimilarity framework,” Ph.D. thesis, Johns Hopkins University.
- Ma, Z., Marchette, D. J., and Priebe, C. E. (2012), “Fusion and inference from multiple data sources in a commensurate space,” *Statistical Analysis and Data Mining*, 5, 187–193.
- Nastar, C., Moghaddam, B., and Pentland, A. (1996), “Generalized image matching: Statistical learning of physically-based deformations,” in *Computer Vision ECCV’96*, Springer, pp. 589–598.
- Pan, S. J. and Yang, Q. (2010), “A survey on transfer learning,” *Knowledge and Data Engineering, IEEE Transactions on*, 22, 1345–1359.
- Park, Y., Wang, H., Nobauer, T., Vaziri, A., and Priebe, C. E. (2015), “Anomaly detection on whole-brain functional imaging of neuronal activity using graph scan statistics,” in *ACM Conference on Knowledge Discovery and Data Mining, Workshop on Outlier Definition, Detection, and Description*.
- Prevedel, R., Yoon, Y.-G., Hoffmann, M., Pak, N., Wetzstein, G., Kato, S., Schrödel, T., Raskar, R., Zimmer, M., Boyden, E. S., and Vaziri, A. (2014), “Simultaneous whole-animal 3D imaging of neuronal activity using light-field microscopy,” *Nature methods*.
- Priebe, C., Marchette, D., Ma, Z., and Adali, S. (2013), “Manifold matching: joint optimization of fidelity and commensurability,” *Brazilian Journal of Probability and Statistics*, 27, 377400.
- Sahami, M. and Heilman, T. D. (2006), “A web-based kernel function for measuring the similarity of short text snippets,” in *Proceedings of the 15th International Conference on the World Wide Web*, ACM, pp. 377–386.

- Schulz, U. (1980), “An alternative procedure for the analysis of similarity data and its comparison to the Idioscal-and Indscal-procedure,” *Lantermann (Eds.), Similarity and choice*, 140–149.
- Sharma, A., Kumar, A., Daume, H., and Jacobs, D. W. (2012), “Generalized multiview analysis: A discriminative latent space,” in *Computer Vision and Pattern Recognition (CVPR), 2012 IEEE Conference on*, IEEE, pp. 2160–2167.
- Shen, C., Vogelstein, J. T., and Priebe, C. E. (2016), “Manifold Matching using Shortest-Path Distance and Joint Neighborhood Selection,” *arXiv preprint arXiv:1412.4098*.
- Sun, M. and Priebe, C. E. (2013), “Efficiency investigation of manifold matching for text document classification,” *Pattern Recognition Letters*, 34, 1263–1269.
- Torgerson, W. S. (1952), “Multidimensional scaling: I. Theory and method,” *Psychometrika*, 17, 401–419.
- Trosset, M. W. and Priebe, C. E. (2008), “The out-of-sample problem for classical multidimensional scaling,” *Computational statistics & data analysis*, 52, 4635–4642.
- Vinokourov, A., Cristianini, N., and Shawe-Taylor, J. S. (2002), “Inferring a semantic representation of text via cross-language correlation analysis,” in *Advances in Neural Information Processing Systems*, pp. 1473–1480.
- Wang, C. and Mahadevan, S. (2008), “Manifold alignment using Procrustes analysis,” in *Proceedings of the 25th International Conference on Machine Learning*, ACM, pp. 1120–1127.
- (2009), “Manifold Alignment without Correspondence.” in *IJCAI*, vol. 2.
- Wang, L. and Suter, D. (2007), “Learning and matching of dynamic shape manifolds for human action recognition,” *Image Processing, IEEE Transactions on*, 16, 1646–1661.
- Woodbury, M. A. (1950), “Inverting modified matrices,” *Memorandum report*, 42, 106.